(2)

AFWAL-TR-88-1128

MEGALIDAR

A. K. Garrison, G. W. Grams, E. M. Patterson
and D. W. Roberts

Georgia Institute of Technology
Georgia Tech Research Institute
Electromagnetics Laboratory
Electro-Optics Division
Atlanta, Georgia 30332

February 1989

Interim Report for Period August, 1987 - January, 1988

Approved for public release; distribution unlimited

Avionics Laboratory
Air Force Wright Aeronautical Laboratories
Air Force Systems Command
Wright-Patterson Air Force Base, Ohio 45433-6543

NOTICE

When Government drawings, specifications, or other data are used for any purpose other than in connection with a definitely related Government procurement operation, the United States Government thereby incurs no responsibility nor any obligation whatsoever; and the fact that the government may have formulated, furnished, or in any way supplied the said drawings, specifications, or other data, is not to be regarded by implication or otherwise as in any manner licensing the holder or any other person or corporation, or conveying any rights or permission to manufacture use, or sell any patented invention that may in any way be related thereto.

This report has been reviewed by the Office of Public Affairs (ASD/PA) and is releasable to the National Technical Information Service (NTIS). At NTIS, it will be available to the general public, including foreign nations.

This technical report has been reviewed and is approved for publication.

JAN SERVAITES, AARI-3
Project Engineer
EO Sensors Eval/Analysis Group
Electro-Optics Branch

JAMES J. STEWART, CHIEF, AARI-3
EO Sensors Eval/Analysis Group
Electro-Optics Branch

FOR THE COMMANDER

GALE D. URBAN, Chief
Electro-Optics Branch
Mission Avionics Division

If your address has changed, if you wish to be removed from our mailing list, or if the addressee is no longer employed by your organization please notify WRDC/AARI-3 *W-PAFB, OH 45433 to help us maintain a current mailing list.*

Copies of this report should not be returned unless return is required by security considerations, contractual obligations, or notice on a specific document.

SECURITY CLASSIFICATION OF THIS PAGE

REPORT DOCUMENTATION PAGE

Form Approved OMB No. 0704-0188

1a. REPORT SECURITY CLASSIFICATION UNCLASSIFIED	1b. RESTRICTIVE MARKINGS
2a. SECURITY CLASSIFICATION AUTHORITY	3. DISTRIBUTION/AVAILABILITY OF REPORT Approved for public release; distribution is unlimited.
2b. DECLASSIFICATION/DOWNGRADING SCHEDULE	
4. PERFORMING ORGANIZATION REPORT NUMBER(S)	5. MONITORING ORGANIZATION REPORT NUMBER(S) AFWAL TR-88-1128
6a. NAME OF PERFORMING ORGANIZATION Georgia Tech Research Inst. — 6b. OFFICE SYMBOL (If applicable)	7a. NAME OF MONITORING ORGANIZATION Avionics Laboratory (AFWAL/AARI) AF Wright-Aeronautical Laboratories
6c. ADDRESS (City, State, and ZIP Code) Georgia Institute of Technology Atlanta GA 30322	7b. ADDRESS (City, State, and ZIP Code) Wright-Patterson AFB OH 45433-6523
8a. NAME OF FUNDING/SPONSORING ORGANIZATION — 8b. OFFICE SYMBOL (If applicable)	9. PROCUREMENT INSTRUMENT IDENTIFICATION NUMBER Contract No. F33615-86-C-1051 TA NO 87-5-4
8c. ADDRESS (City, State, and ZIP Code)	10. SOURCE OF FUNDING NUMBERS PROGRAM ELEMENT NO. 61101F — PROJECT NO. ILIR — TASK NO A7 — WORK UNIT ACCESSION NO. 06
11. TITLE (Include Security Classification) MegaLIDAR	
12. PERSONAL AUTHOR(S) A K Garrison, G W Grams, E W Patterson, D W Roberts	
13a. TYPE OF REPORT — 13b. TIME COVERED FROM 8/1/87 TO 1/31/88 — 14. DATE OF REPORT (Year, Month, Day) 1989 February 08 — 15. PAGE COUNT 89	
16. SUPPLEMENTARY NOTATION	

17. COSATI CODES			18. SUBJECT TERMS (Continue on reverse if necessary and identify by block number)
FIELD	GROUP	SUB-GROUP	
04	01		LIDAR, Remote Sensing, Collimator, telescope, Raman, Ozone, Rayleigh Scatter, Mesosphere, Atmosphere Density, NASP

19. ABSTRACT (Continue on reverse if necessary and identify by block number)

This interim report is the result of an investigation of the applicability of the 100-inch collimator facility to a LIDAR measurements program for AFWAL/AARI-3 at Wright-Patterson AFB. Particular measurements of atmospheric parameters and phenomena are suggested. The performance of the 100-inch LIDAR for observing Rayleigh and Raman backscattering from various altitudes were simulated assuming different laser powers and signal averaging times and the results are presented and discussed. A review of the kinds of LIDAR measurements that are required for broad coverage of atmospheric phenomena as well as a review of the technology required to instrument these measurements are given. The current status of the collimator is summarized and changes in the collimator optics to accomodate a 10.6-micrometer LIDAR are suggested. Preliminary designs for transmitter and receiver modules to facilitate the use of the collimator as a multi-LIDAR facility are discussed.

20. DISTRIBUTION/AVAILABILITY OF ABSTRACT ☒ UNCLASSIFIED/UNLIMITED ☐ SAME AS RPT. ☐ DTIC USERS	21. ABSTRACT SECURITY CLASSIFICATION UNCLASSIFIED
22a. NAME OF RESPONSIBLE INDIVIDUAL Mr Jan M. Servaites	22b. TELEPHONE (Include Area Code) 513/255-9609 — 22c. OFFICE SYMBOL AFWAL-AARI-3

DD Form 1473, JUN 86 — Previous editions are obsolete.

PREFACE

This Interim Report summarizes the efforts performed during the period from 1 August 1987 to 31 January 1988, by Georgia Tech Research Institute for AFWAL/AARI-3 under contract number F33615-86-C-1051, Task 87-5-4 from the Avionics Laboratory, Air Force Wright Aeronautical Laboratories (AFWAL).

Sponsor for the project is the EO Sensor/Atmospheric Science Group (AARI-3) of the Avionics Laboratory. The technical monitor at AFWAL is Lt. Mario Moya. He is supported by the MegaLIDAR Project Engineer Mr. Jan Servaites.

Participants at GTRI, in addition to the authors, include Dr. R. S. Hyde, Systems Analysis Branch Head, Ms. Suzanne West, Branch Secretary, and Dr. G. G. Gimmestad. Mr. S. S. Steadman is project director of the GTRI EOS/ATR Sciences Development Program which was the umbrella for this task. Dr. Allen K. Garrison was the principal investigator. The EOS/ATR Sciences Development Program is conducted in the Electro-Optics Division, Mr. David E. Schmieder, Chief, of the Electromagnetics Laboratory, Mr. Devon G. Crowe, Director.

TABLE OF CONTENTS

TABLE OF CONTENTS (Cont'd)

LIST OF FIGURES

LIST OF TABLES

I. Introduction

This report is about the fortunate conjunction of the need for crucial information and the existence of a superb facility that can meet the need with an expenditure amounting to a fraction of the original cost of the facility. The needed information is an accurate determination of the spatial and temporal variations of the parameters that characterize the atmosphere from 30 to 60 km. This region of the atmosphere is sometimes referred to as the "ignoredsphere" because so few measurements have been made in the range. This information is crucial to the Air Force because it is a region where future operations will take place and thus cannot remain unknown and unexplored. The facility that will form the basis of the program to supply the crucial information is the 100-inch optical collimator housed in the AARI building at Wright-Patterson Air Force Base. The features of this facility, which are not duplicated anywhere else in the world, form a basis for the development of an unexcelled measurements program for this region of the atmosphere. The connection between the collimator and the atmospheric measurements is the use of a powerful remote sensing technique that is called LIDAR (Light Detection and Ranging). Thus, the facility has been designated the MEGALIDAR Facility and the measurement program the MEGALIDAR Program.

Tables 1 and 2 show that the 100-inch collimator can be a truly MEGALIDAR. Table 1 lists some of the characteristics of LIDAR facilities around the world that have been given in the remote sensing literature as well as those that the MEGALIDAR will have. The wavelength, pulse energy and pulse rate are parameters of the laser transmitter and the detection efficiency is an important receiver specification. Table 2 offers a more succinct and accurate comparison by using a figure of merit that assesses the relative range, accuracy and data rates of the various LIDARS. This comparison shows that the 100-inch collimator will indeed be a world class LIDAR.

The report first discusses specific measurements that are recommended for their support of Air Force programs and

establishes the place of the MEGALIDAR in the LIDAR community. This is followed by Section III on LIDAR performance requirements including simulations of the performance of the MEGALIDAR. The principal aim of this section is to justify the development of a multi-laser capability for the MEGALIDAR. Section IV characterizes the available instrumentation and examines some of the design criteria for implementing the measurements and performance discussed in Sections II and III. Section V adds a discussion of the design of the optical systems for the various LIDARs and how they can be adapted to the MEGALIDAR. Section VI reviews the current status of the 100-inch collimator and describes some of its unique features.

Table 1. COMPARISON OF MIDDLE ATMOSPHERE LIDAR FACILITIES

LOCATION	MIRROR D(cm)	WAVELENGTH (microns)	ENERGY/PULSE E(Joules)	PULSE RATE P(Hz)	DETECTION EFFICIENCY e
JAPAN	167.0	1.06	1.2	25	0.08%
		0.532	0.4	25	15%
FRANCE	81.8	0.589	1.0	1	15%
	60.0	0.532	0.3	10	15%
(maritime-mobile)	50.0 X 8(eight receivers)	0.532	0.3	10 X 7 (seven lasers used in sequence)	15%
W. GERMANY	150.0	0.589	0.01	10	15%
USA (AFGL penthouse)	91.4	0.532	0.4	10	15%
USA (AFGL mobile)	60.9	0.351	0.3	60	15%
USA (Wright-Patterson AFB)	254.0	1.06	0.6	30	2%
		0.532	0.22	30	15%

Table 2. Figure of Merit

$$M = \frac{A\ E\ P\ e}{\lambda^4}$$

	M (0.351 microns)	M (0.5 microns)	M (1.06 microns)
JAPAN		410	0.4
FRANCE		6	
		15	
(maritime-mobile)		617	
W. GERMANY		2	
USA (AFGL penthouse)		49	
USA (AFGL mobile)	518		
USA (Wright-Patterson AFB)		626	14

II. Atmospheric Phenomena and Parameters Amenable to LIDAR Measurements

A. Cloud Characterization Studies

A set of Air Force needs concerns a better determination of the radiative effects of clouds, particularly cirrus clouds, on E-O systems (Bauer, et al, 1984). These clouds can affect E-O system performance by reducing the transmission between a source and a detector, by increasing path and background radiance values, and by clutter of the background radiation seen by detectors. Cirrus clouds, for example, can contribute to the anomalous sky radiance levels that have been seen in the atmospheric window regions (Schmidt, 1988); they can also significantly reduce IR sensor performance (Abel, et al, 1986). The problem is particularly acute because significant optical effects can be produced by subvisual cirrus for which there are no adequate characterization studies or concentration statistics at present.

In addition, the increasing importance of E-O systems in today's Air Force requires an ability to predict cloud effects for various scenarios. Thus, E-O system development requires improved capabilities for modeling the radiative effects of clouds, particularly thin cirrus clouds, for the different wavelengths of optical interest. There is also the need for a better capability to model the expected effects of clouds on E-O systems based on standard meteorological data. The 100-inch LIDAR facility will have a capability for long-term cloud characterization and studies that is not matched by any other facility.

Cloud characterization for studies of radiative effects requires, at a minimum, determination of the attenuation coefficient and the light scattering properties of the clouds as a function of wavelength. A detailed measure of the amount of near forward scattered light, with an indication of the angular variation close to the 0 scattering angle, as well as direct measurements of the radiance of these clouds as functions of wavelength are also desirable additional information. Although a

vertically pointing LIDAR cannot make a complete characterization, if simultaneous measurements of extinction and backscatter are made, then this data can constrain models of cloud effects sufficiently so that the other properties can be inferred.

The direct measurement of the radiative properties of these clouds is based on very few measurements (see, e.g. Post, 1984). Similarly, modeling efforts predicting cloud properties from standard meteorological observables have also been based on a very limited data base. While many presently available LIDAR systems can measure backscatter from cirrus clouds and can be used to determine occurrence and thickness statistics, most ground based LIDAR systems cannot do characterization because they do not have the sensitivity to make routine measurements of the attenuation of the backscatter signal from particles higher than the clouds. The proposed 100-inch LIDAR facility will have the needed sensitivity to make such measurements.

To perform the cloud characterization studies, we recommend two laser systems, a Nd:YAG system operating at 1.06, 0.53 and 0.35 micron wavelengths, and a CO_2 system operating at 10.6 μm wavelength. An infrared radiometer should be used as an auxiliary measurement. Backscatter coefficients would be determined for cirrus clouds at the four wavelengths. Attenuation coefficients would be determined by analyses of decrease in stratospheric return by the clouds with sufficient optical depth for measurable attenuation of higher scattering returns. We estimate that useful data will be obtained for clouds with total optical depths of 0.05 or greater. Effects of less attenuating clouds would be determined by analysis of backscatter values at the different wavelengths. Infrared emission data will be used as a surrogate for optical depth in the analysis for less attenuating clouds. A possible later modification of the experiment would involve the addition of a capability to vary the field of view of the LIDAR to accept varying amounts of multiple scattered light from the thicker clouds. Simultaneous or near simultaneous radiosonde data would be used to determine temperature and water vapor profiles.

This discussion outlines the uses of the 100-inch LIDAR system in cloud studies. Simple cloud climatology studies are not emphasized because we feel that the 100-inch system is most useful for detailed studies in which the sensitivity of the system is used to provide data to interpret other basic climatology studies. While measurements of cloud climatology can be usefully made on the 100-inch system, these measurements can also be made on much smaller systems, and so should have a lower priority on the 100-inch system.

We would also emphasize that these cloud characterization measurements should be made as one part of a coordinated research program that also includes cloud microphysical models to relate cloud and radiative characteristics, cloud climatology measurements and analyses, and development of a predictive scheme for forecasting effects of cirrus on E-O system performance on a global basis.

B. Upper Stratospheric and Mesospheric Aerosols

Although there is a large body of data on the aerosols in the lower stratosphere, there is little data above 30 km because of the limitations of most LIDAR systems. The data is of interest because of the possible effects of aerosols on propagation of high energy electromagnetic pulses in the upper atmosphere, which are primarily determined by aerosol absorption. The aerosols are also useful as a tracer of atmospheric motions and structure functions, providing data which can help to understand the dynamics of the upper atmosphere.

The most widely used models of the upper atmospheric aerosol above 30 km are those of the AFGL that are used in the LOWTRAN program (Kneizys, et al, 1980). In this program the choice of two upper atmospheric models is given, one for a "normal" aerosol and one for an "extreme" aerosol. For altitudes of more than 30 km, the models differ only in the assumed aerosol concentration. Both are assumed to be composed of meteoric dust with a constant size distribution. The models are based on very few measurements and no indication of the relative importance of the extreme

concentration model is given. A cursory examination of a portion of the SAGE data set (McCormick, 1986) suggests that the normal aerosol model is appropriate in the altitude range of 30 to 40 km. Other data such as that of Fiocco and Grams (1969), or that determined by the Solar Mesosphere Explorer (Barth, 1983), suggests significantly higher concentrations in discrete layers above 30 km.

The suitability of the 100-inch LIDAR system to measure these layers can be seen from Figures 1 and 2 for backscatter at 1.06 and 10.6 μm respectively. In each of these figures the aerosol backscatter (β) values are determined as a function of altitude by scaling the AFGL mode altitude profiles, which are given for 0.55 μm, to the wavelength of interest and using the AFGL extinction, absorption, and phase function models to infer a β value. In Figure 1 for 1.06 data, the β for Rayleigh scattering are shown as a dashed line; the normal aerosol line and the extreme aerosol are shown as solid lines. The normal aerosol appears to have a scattering ratio of roughly 0.4 for the altitudes between 40 and 100 km. The enhanced aerosol can be an order of magnitude higher than Rayleigh scattering. In Figure 2 for 10.6 μm, data curves are the same as in Figure 1. Due to the long wavelength, the molecular scattering is relatively much smaller than the aerosol returns. The sensitivity of a nominal heterodyne CO_2 system is shown as the dotted line in Figure 2. This sensitivity was estimated from the sensitivity of the NOAA system as given by Post (1984) with scaling to the parameters of the 100-inch receiver. The laser was assumed to have an output power of 2 J/pulse with data based on 5000 pulse averages.

Experimentally, we would recommend that the measurements be done with the 1.06, 0.53, and 0.35 micron wavelengths of the Nd:YAG laser. An analyses using the fundamental and tripled wavelengths as described in Russell, et al (1981), makes use of the differing wavelength dependence of molecular and aerosol returns to separate the molecular and aerosol components. We expect that the tripled wavelength data will be almost completely determined by the molecular return, while the longer wavelength

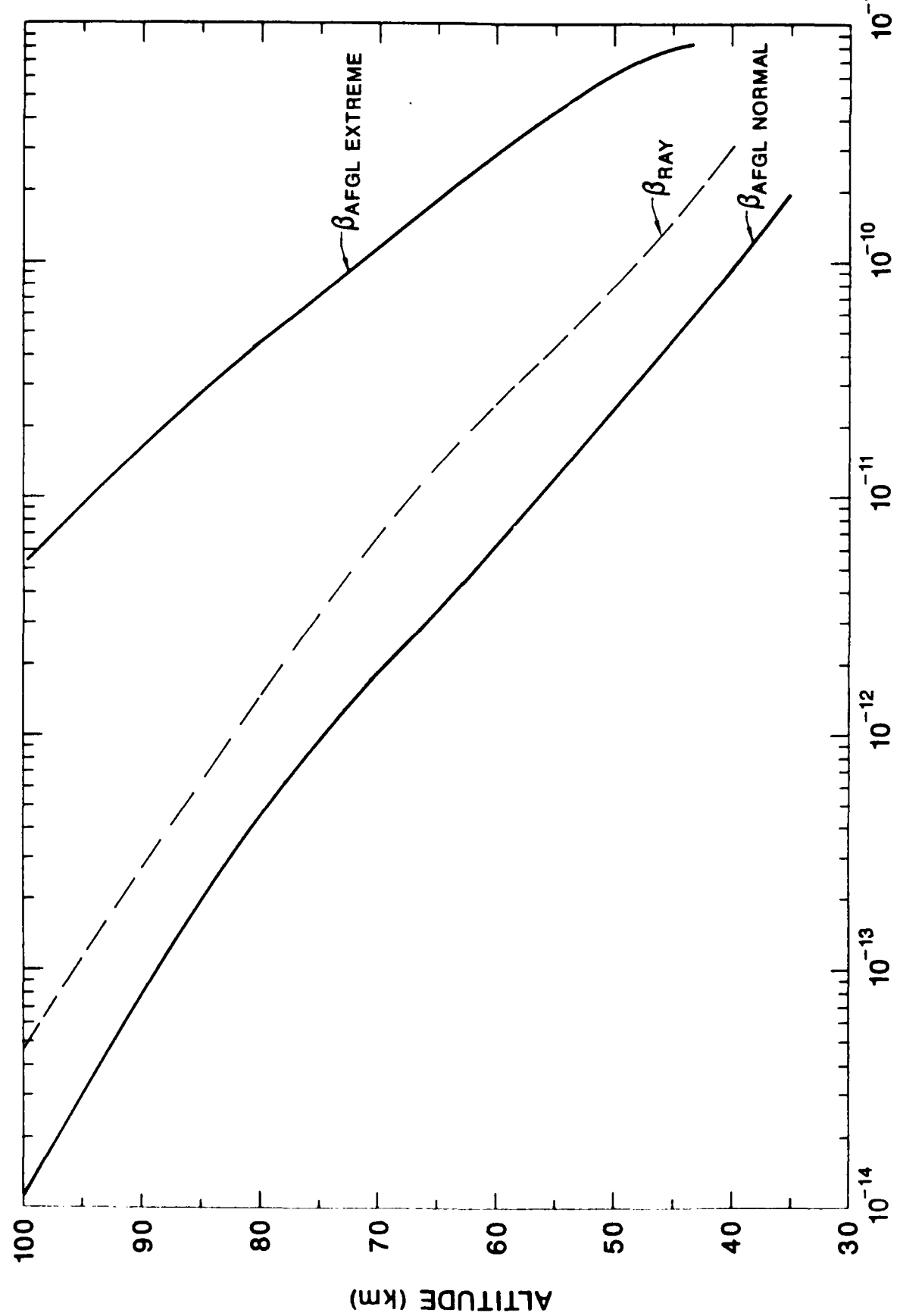

Fig. 1. Backscatter at 1.06 μm

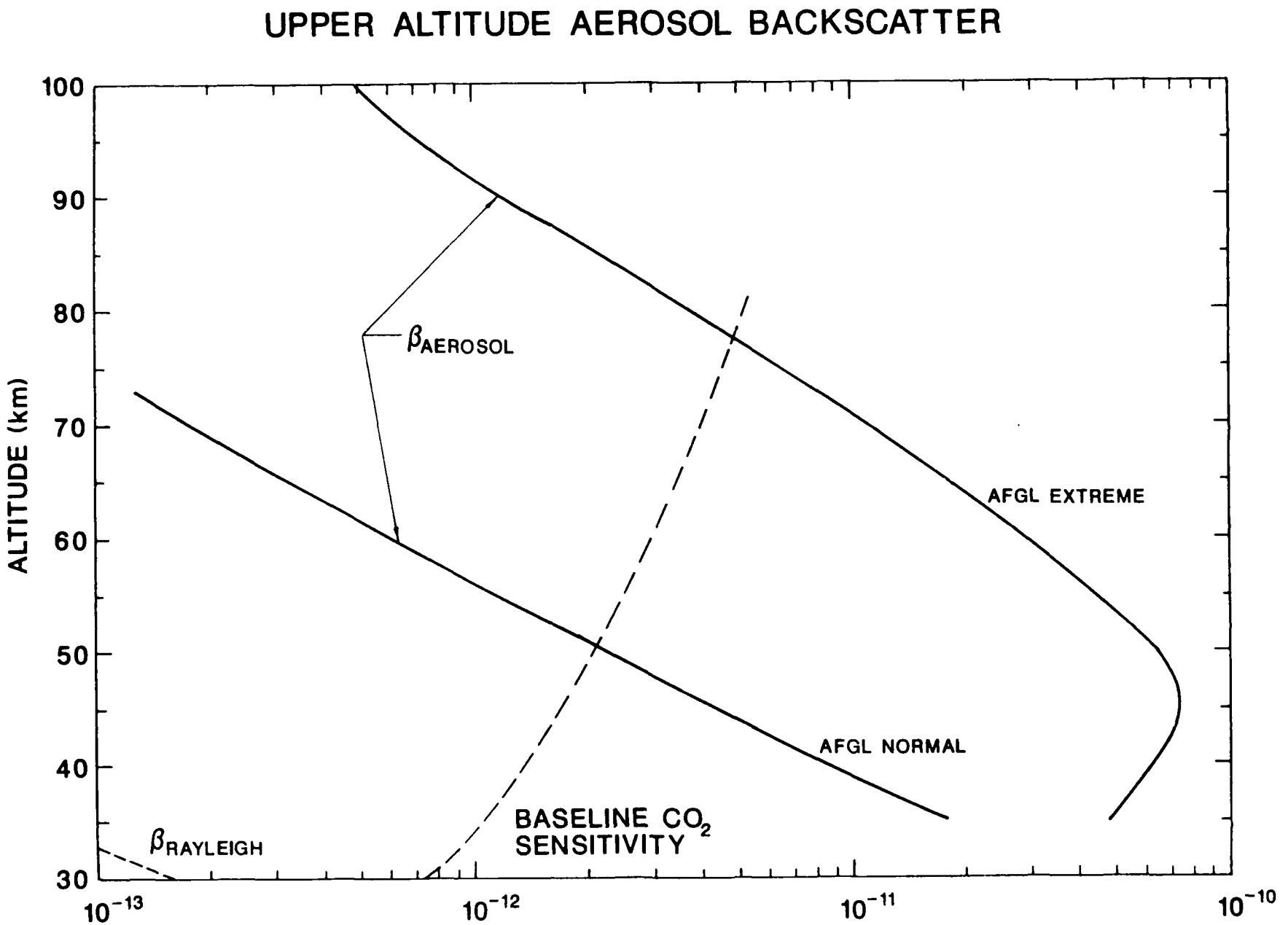

Fig. 2. Backscatter at 10.6 μm

returns will have a more significant aerosol component. For additional information on the effects of the aerosol at longer wavelengths, a heterodyne CO_2 system would be useful for altitudes up to approximately 50 km. Measurements in conjunction with wind measurements (i.e., such as that provided by meteor wind radar) could provide aerosol and atmospheric structure function information. Modeling of aerosol characteristics would be needed to interpret the backscatter data in terms of attenuation and absorption and to estimate size distributions from backscatter data.

C. Ozone Concentrations

Possible depletion of the ozone layer due to anthropogenic activities has become a topic of national concern. In addition, the determination of the ozone concentration is a very important measurement for different air chemistry studies. There are currently two basic approaches to determination of ozone concentration on a global basis, a set of ground based spectrophotometer measurements and different satellite instruments. Each of the approaches has limitations, due in large part to the need to invert radiation data from passive sensors. Because of the inherent limitations of the data and because of differences in the data sets, direct measurements of the ozone are needed to aid in the interpretation of the passive remote sensing data.

Differential absorption LIDAR (DIAL) (see Section III) systems have been used to determine ozone concentrations to altitudes of between 25 and 30 km. The rationale for the use of a DIAL system is shown in Figure 3 from Patterson and Gillespie (1987) which is a plot of attenuation versus wavelength at standard conditions for ozone absorption (__ _ _ __), aerosol attenuation (.....), molecular oxygen absorption (__ __ __), and molecular scattering (_._._.). Solid lines total atmospheric attenuation. The change in the ozone attenuation with wavelengths near 300 nm is much greater than the change in either aerosol or molecular attenuation. The measurements are made by

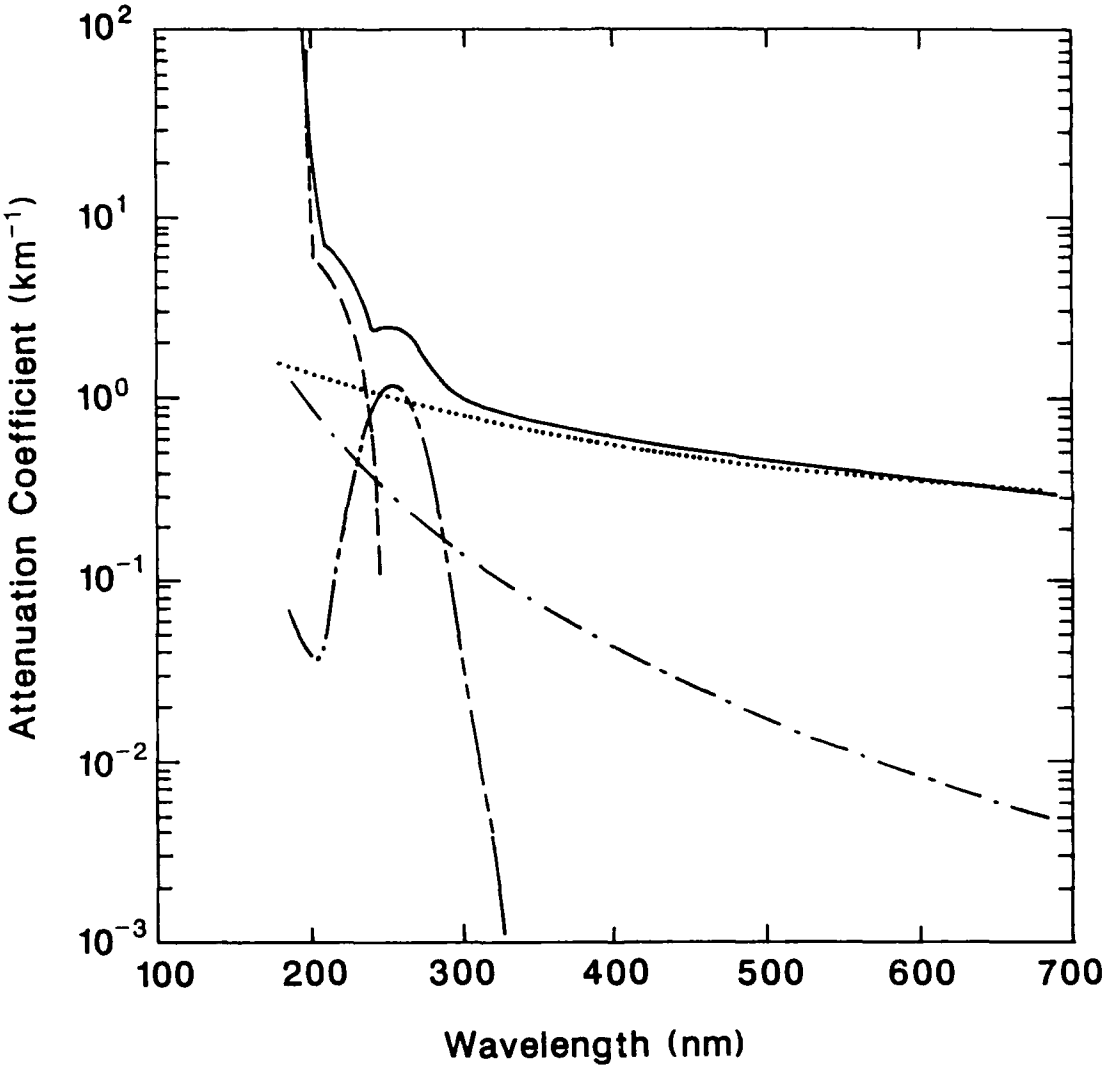

Fig. 3. Modeled Attenuation for Ozone DIAL

probing the atmosphere with two closely spaced wavelengths, an "on-line" wavelength that is strongly affected by the absorption line and an "off-line" wavelength that is affected by the scattering only. The differential absorption at the two wavelengths produces a difference in signal from which the ozone concentration as a function of altitude can be determined.

Browell (1982), of Langley Research Center, and Uchino, et al (1979) of Kyushu University, Japan, have used different variations of the differential absorption technique to determine ozone concentrations. Browell used frequency doubled dye systems pumped by doubled Nd:YAG systems, and Uchino used a XeCl excimer system at 308 nm for the on-line wavelength that was referenced against aerosol backscatter extrapolated from 530 nm. Current systems, however, do not have the sensitivity to measure throughout the ozone layer, particularly at higher altitudes at which some models predict that ozone concentration changes would first be seen.

We are proposing a program of measurements of the ozone concentration by means of a DIAL system consisting of a XeCl excimer laser operating at 308 nm as the on-line channel and a frequency tripled Nd:YAG system at 353 nm as the off-line channel. Doubled and fundamental Nd:YAG systems at 530 and 1060 nm would also be used to extrapolate the 353-nm data to 308 in the absence of ozone absorption effects. Standard DIAL analyses techniques would be used. This proposed system would have the sensitivity to measure ozone concentrations to well above 30 km.

This series of measurements would provide a continuous record of ozone concentrations at one site. More importantly, it would provide ground truth data for different satellite measurement programs. In addition, other channels could be added for comprehensive measurements of other possibly interfering constituents as a means of verifying satellite inversion algorithms. Such additional measurements would be done subsequent to the initial basic ozone measurements.

D. Density and Temperature Profiles

Density and temperature profiles in the altitude range 35 km to 90 km can be obtained with a ground based LIDAR system operating in the visible wavelength region. The LIDAR returns are analyzed to obtain volume backscattering coefficients. The coefficient is a single number that depends on the number density of the molecular constituents in the path and the kind of scattering that takes place - Rayleigh or Mie. To obtain the number density, we must determine the contribution to the back-scattering from aerosols. This can be done experimentally by obtaining the backscattering coefficient with at least two wavelengths and using the fact that the Rayleigh backscattering cross section depends on the fourth power of the reciprocal wavelength. Thus, the aerosol contribution to the volume backscattering coefficient can be identified and removed from the backscattering data. Once the Rayleigh contribution is known then it can be assumed that this comes primarily from air molecules whose back-scattering cross sections are well known and the number density and hence the mass density can be calculated. Since the LIDAR gives backscattering coefficients as a function of height, the density profile can be obtained.

If a multiple wavelength system is not available, then the partition of the backscattering coefficient must be done by assuming some model. In the 35- to 70-km altitude range, it is sometimes assumed that the aerosol backscattering coefficient is zero.

The temperature profile can be obtained from the mass density profile by assuming the atmosphere obeys the ideal gas law and is in hydrostatic equilibrium so that the changes in pressure with altitude can be described by the barometric equation. It is also assumed that the atmospheric turbulence does not affect the mean density at the level of the spatial and temporal resolution obtained by the LIDAR.

Uncertainties in the laser power, atmospheric transmission and the electro optical efficiency of the LIDAR system prevent

the measurements from being absolute. Thus, it is necessary to normalize the density profiles using an absolute profile from a model or other experimental data. It is also necessary to fit the pressure profile at one altitude with a value from an independent source.

E. Atmospheric Molecular Scattering Profiles

We have calculated the backscattered signals that are expected for air molecules illuminated by the laser beam on the 100-inch system. The signals are presented in terms of the number of photoelectrons that would be observed in a fixed time interval for a system that incorporated a frequency-doubled Nd:YAG laser operating at a rate of 20 pulses per second with 0.5 joule pulses at 0.53 μm wavelength. In addition, it is assumed that the efficiency for the transmitter optics is 20 percent and for the receiver optics, including an interference filter, is 40 percent, and that the quantum efficiency of the photomultiplier tube is 20 percent at 0.53 micrometers (see Section III). It must be emphasized that these calculations are for the number of photoelectrons per measurement interval produced by the returning photon flux and do not include noise produced by any source such as background or detector. Thus, this is an ideal number that actually cannot be recorded. The equivalent number of photoelectrons produced by noise sources must be estimated and compared with the calculations to obtain an estimate of the actual performance of the MEGALIDAR.

For a vertically pointing LIDAR, altitude is determined by the round-trip time interval after the laser was pulsed. For a range resolution element of any given length, we multiply its round-trip travel time (6.6 μsec/km) by the instantaneous rate of arrival of photons from the altitude of interest to determine the number of photons expected from that range interval. Figure 4 shows an example of one of our calculations. It refers to a system incorporating the 100-inch collimator mirror and a Nd:YAG laser with a 0.5-joule pulse at the wavelength of 0.53 μm. The

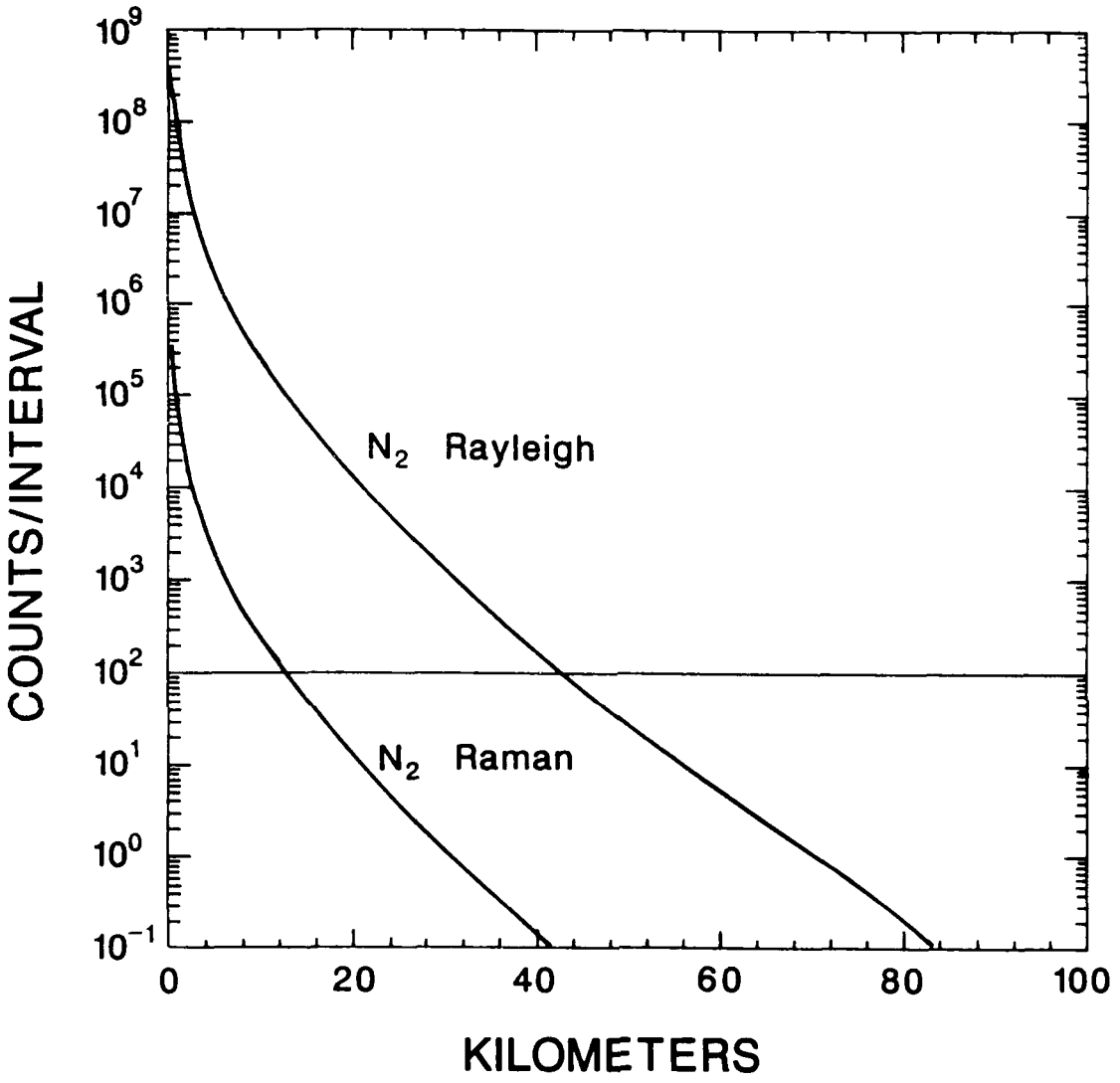

Wavelength = 0.53 microns
Energy per pulse = 0.5 Joules
Counts for single pulse

Receiver diameter = 100 inches
Range interval = 0.15 km

Fig. 4. Simulation of Backscattered Counts / Interval versus Range for MEGALIDAR

range interval is taken to be 150 m (counts observed in 1 μsec time intervals). Very high count rates are obtained at the lower altitudes. The horizontal line drawn at 100 counts per sample interval indicates the altitude at which the photoelectron rate has dropped to a value where statistical fluctuations of the signal will begin to dominate signal-to-noise calculations. (This assumes background counts are less than 100 counts per sample interval.) At higher altitudes, signal averaging techniques must be applied to a series of consecutive pulses to obtain useful results. The thick curve on the figure represents Rayleigh scattering by atmospheric molecules with the U.S. Standard Atmosphere (1962) density profile; the figure shows that single-pulse density observations can be made to about 40 km with the MEGALIDAR system. The thin curve represents the corresponding signals due to Raman scattering (see Section III) by nitrogen molecules; the figure shows that single-pulse nitrogen profiles can be measured to about 15-km altitude.

In actual operation, a LIDAR system with a high pulse rate laser such as the Nd:YAG system used for the present calculations would use a transient recorder incorporating a signal averager to record and analyze the average echo for a given number of pulses to improve the signal-to-noise ratio and, thereby, to increase the maximum altitude for obtaining useful observations (see Section IV). For example, Figure 5 shows the results of operating a signal averager for a 1-minute time interval with a 20-pulse/second Nd:YAG laser. Under these conditions, the average signal would be based on a summation of 1200 pulses so that the number of counts summed in each altitude interval would increase by that factor. In this case, the altitude associated with the 100-count sum is found at about 85 km for Rayleigh scattering and about 40 km for the nitrogen Raman signal (assuming 100 background counts).

Since the mid-latitude stratospheric aerosol layer peaks in the 15- to 20-km altitude range and decreases to negligible fractions of the molecular scattering profile at 30 km and above, the 1-minute average profiles would include Raman nitrogen profiles,

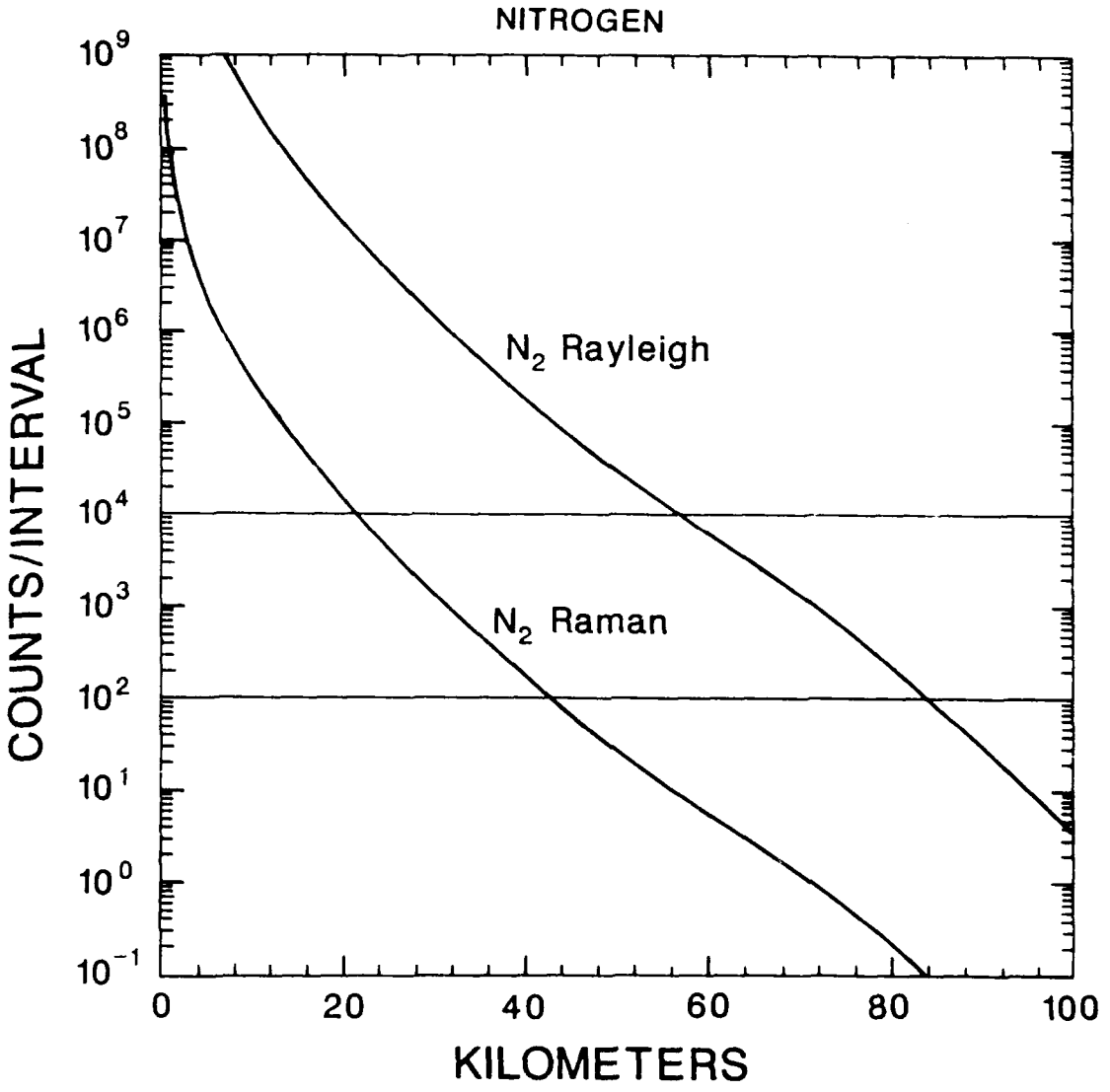

Wavelength = 0.53 microns
Energy per pulse = 0.5 Joules
Pulse rate = 20 per second
Observation time = 1 minute
Receiver diameter = 100 inches
Range interval = 0.15 km

Fig. 5. Simulation of Backscattered Counts / Interval versus Range for MEGALIDAR

unadulterated by aerosol scattering, to altitudes that extend to some 10 km above the regions for which the aerosol layer can cause excess scattering contributions. Furthermore, the scattering at the laser wavelength would be expected to be pure Rayleigh scattering from 30 km and above. The combination of nitrogen profiles to 40 km and pure Rayleigh profiles from about 30 to 80 km with 150-m altitude resolution on a minute-to-minute basis represents the unique new contribution that a MEGALIDAR can make to the study of the dissipation of gravity waves and turbulence in the middle atmosphere.

The studies of the sodium layer by the University of Illinois LIDAR group show that the vertical wavelengths of gravity waves in the 80-100 km region are of order 2 or 3 km. Figure 6 shows the results of our computer simulations for a 1-minute observation with 1-km vertical resolution. We see that the trade-offs offered by using a degraded range resolution will push the maximum altitude for the 1-minute average to over 90 km for the Rayleigh and 50 km for Raman signals.

Atmospheric tidal motions are also of interest to the MEGALIDAR program. The observations of tides over the LIDAR system operated in Jamaica (G. S. Kent, et al, 1971) in the late 1960s showed signals obtained with 5 km vertical resolution and approximately 1 hour temporal resolution with greater than 1 percent variations observed above 60 km, increasing to 10 or 20 percent at 100-km altitude. The MEGALIDAR is capable of seeing such variations with much higher spatial and temporal resolution. For example, Figure 7 shows calculations for a 1-hour average signal with 1-km vertical resolution. The summations exceed 100 counts per 1-km interval at the highest altitude displayed on the figure (100 km). Referring back to Figure 6, we see that even the minute-by-minute observations will have signal to noise values that approach the requirements for the tidal studies (1 percent for 60 km, 10 percent at 90 km). Since the tidal studies in the past have emphasized the diurnal and semi-diurnal components, it is clear that the MEGALIDAR will be able to study those components with higher accuracy than obtained in the past

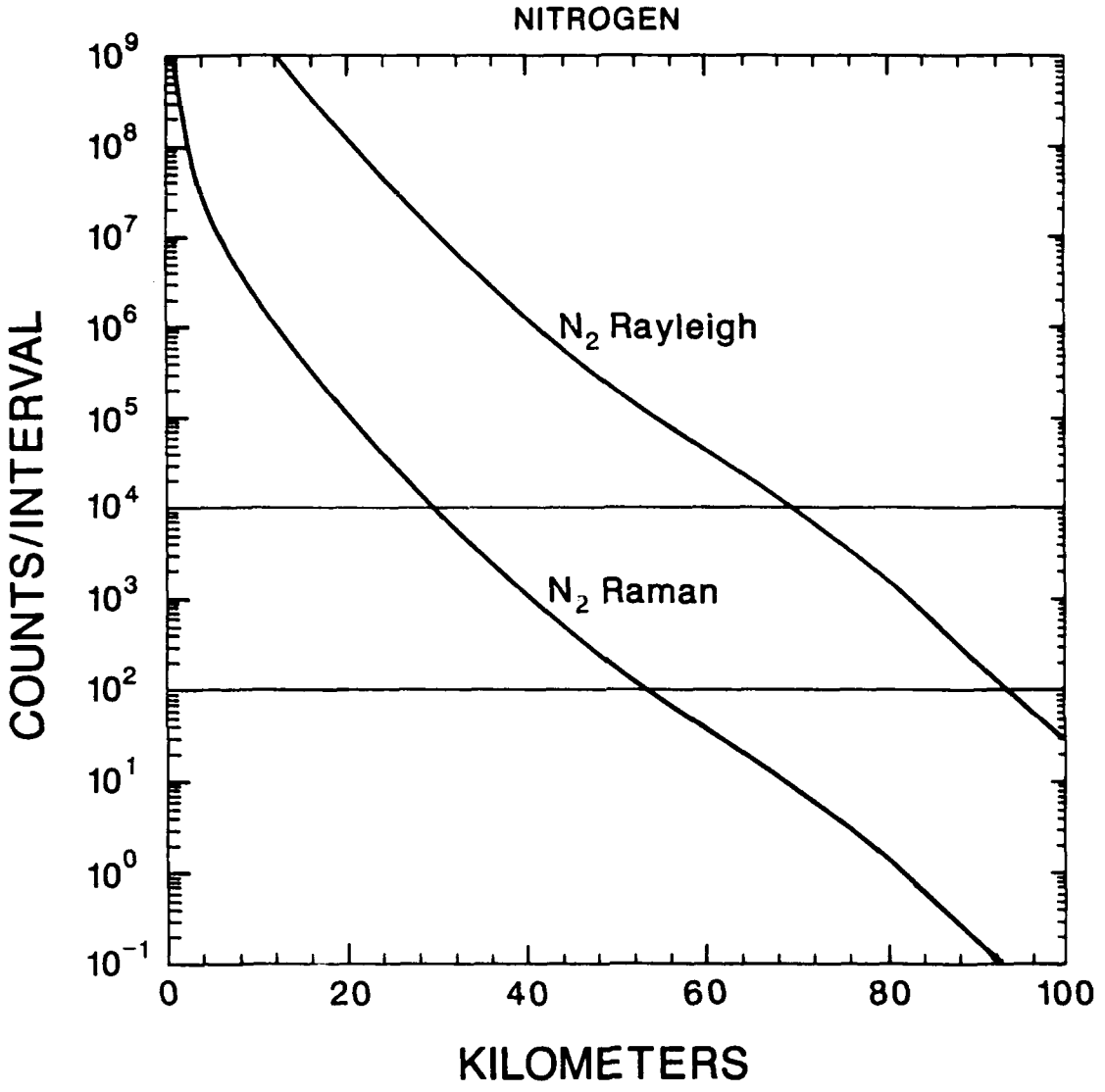

Wavelength = 0.53 microns
Energy per pulse = 0.5 Joules
Pulse rate = 20 per second
Observation time = 1 minute
Receiver diameter = 100 inches
Range interval = 1 km

Fig. 6. Simulation of Backscattered Counts / Interval versus Range for MEGALIDAR

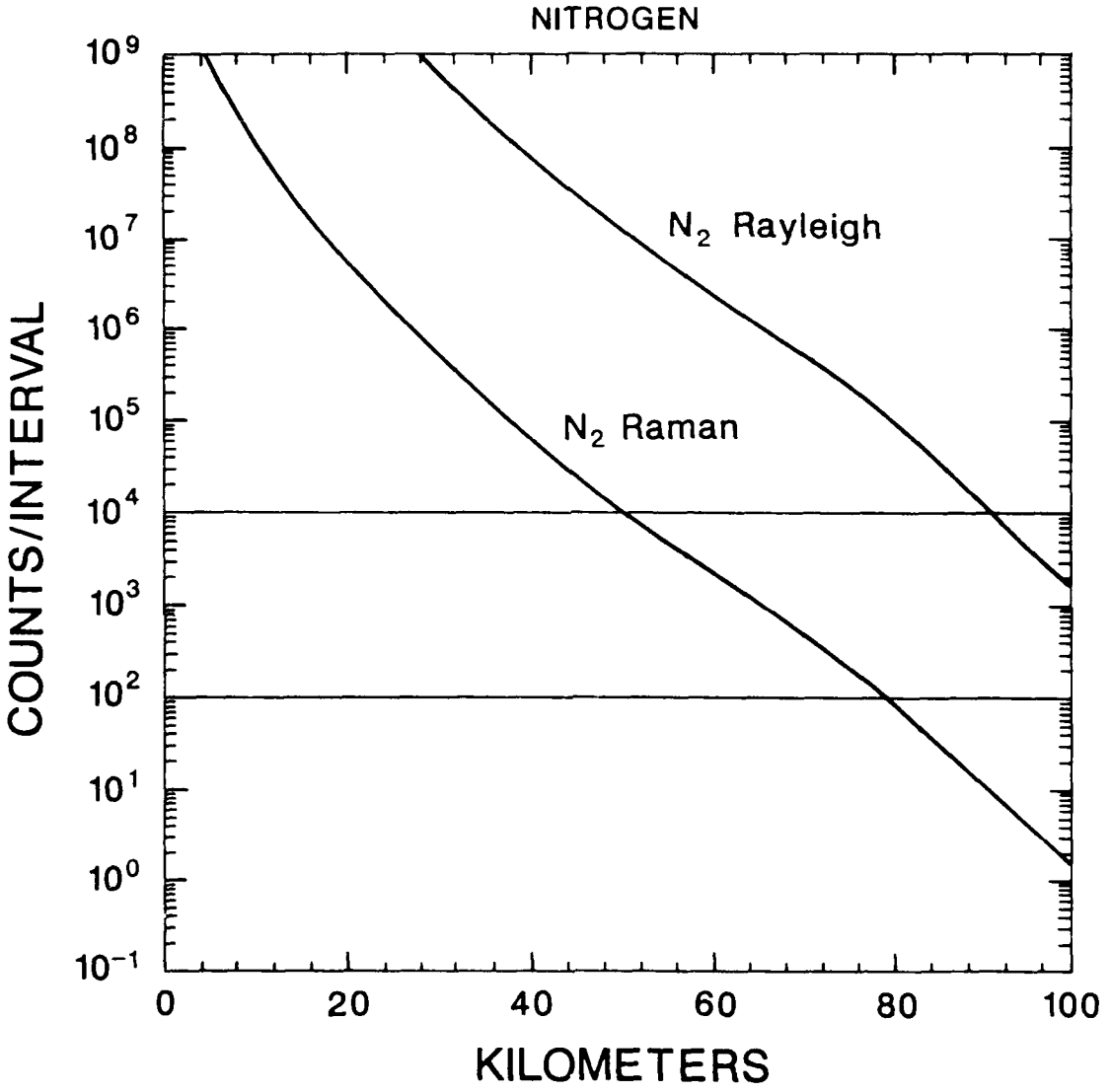

Wavelength = 0.53 microns
Energy per pulse = 0.5 Joules
Pulse rate = 20 per second
Observation time = 1 hour
Receiver diameter = 100 inches
Range interval = 1 km

Fig.7. Simulation of Backscattered Counts / Interval versus Range for MEGALIDAR

studies and, perhaps, may also offer opportunities to study higher frequency components of the atmospheric tides.

F. Spatial and Time Variation of Temperature and Molecular Density of the Middle Atmosphere

An issue of special importance to operations in the stratosphere, mesosphere, and lower thermosphere is the problem of atmospheric turbulence. Considerable temporal and spatial variations in the intensity of turbulence result from the breakdown of upward propagating gravity waves in those regions. The processes responsible for turbulence generation and variability in the middle atmosphere are just beginning to be addressed with sufficient detail for us to try to understand and predict the processes. The use of the 100-inch collimator would provide new data with heretofore unavailable spatial and temporal resolution for detailed gravity wave and turbulence observations. Such a system could provide direct observations of atmospheric density fluctuations to heights up to 100 km. The density data could also be analyzed to obtain temperature profiles in the stratosphere, mesosphere, and lower thermosphere.

Our approach in this proposed use of the facility would be to analyze the MEGALIDAR data by comparing temperature and density observations to state-of-the-art models of the dynamics of the upper atmosphere to validate and improve those models.

An obvious goal of a research program that combines models and observations would be to develop a predictive capability for monitoring turbulence intensities in the upper atmosphere as a function of height and time. The importance of gravity waves in middle atmosphere dynamics was first recognized by Hines (1960). Recent studies (Houghton, 1978; Lindzen, 1981) suggest that the transport of energy and momentum by gravity waves from lower regions of the atmosphere applies a substantial drag on the mean zonal flow of the mesosphere and lower thermosphere which, in turn, leads to the generation of locally intense turbulence and diffusion in the regions where gravity waves are being dissipated. The turbulence may pose a threat to systems, such as

the space shuttles, which operate in or pass through those regions. Fritts, et al (1985) utilized radar and rocket velocity data to show that turbulence intensities were highly correlated with the phase of the dominant wave motion expected to be the most unstable on the basis of linear saturation theory (Lindzen, 1981; Fritts, et al, 1985). In another study, Fritts and Vincent (1985) found strong evidence for the momentum flux modulation due to large-amplitude tidal motions - suggesting a significant diurnal variability of turbulence intensity with the phase of the atmospheric tidal motions. In studies to date, the turbulence parameters have been measured using radar, balloon or rocket techniques. The use of a large LIDAR system to study atmospheric turbulence would provide unique new data for studying the problem. Unlike balloon or rocket measured profiles, the MEGALIDAR temperature and density observations could be nearly continuous and would permit one to examine the detailed evolution of the gravity wave spectrum. Another advantage for turbulence studies is the fact that MEGALIDAR system observations could extend over a continuous range of altitudes from about 20 to about 100 km whereas the radar systems used previously for turbulence studies do not obtain data in the altitude interval from about 25 to 60 km, which is a critical height range for gravity wave and turbulence studies.

References:

Abel, M. D., R. L. Rodney, E. P. Shettle, 1986, "An estimate of the effects of subvisual cirrus on IRSTS performance," a presentation at Wright-Patterson AFB, OH 45433.

Barth, C., 1983, "Satellite measurements of the El Chichon aerosol cloud during 1982," Paper presented at the XVIII General Assembly of the IUGG, Hamburg, FRG, 15-27 August, 1983.

Bauer, E., L. S. Bernstein, G. M. Weyl, 1984, "Cirrus clouds, some properties and effects on optical systems: a preliminary examination," IDA Paper P-1743, Institute for Defense Analysis, Alexandria, VA 22311.

Browell, E. V., 1982, "Remote sensing of tropospheric gases and aerosols with an airborne DIAL system," Proc. of Workshop on Optical and Laser Remote Sensing, Monterey, CA, Feb 9-11.

Fiocco, G., and G. W. Grams, 1969, "Optical radar observations of mesospheric aerosols in Norway during summer 1966," J. Geophys. Res., 74, 2453-2548.

Fritts, D. C., S. A. Smith, B. B. Balsley and C. R. Philbrick, 1985, "Evidence of gravity wave saturation and local turbulence production in the summer mesosphere and lower thermosphere during the STATE experiment," Submitted to J. Geophys. Res.

Fritts, D. C., and Vincent, 1985, "Mesospheric momentum flux studies at Adelaide, Australia: Observations and a gravity wave/disal interaction model," Submitted to J. Atmos. Sci.

Hines, C. O., 1960, "Internal gravity waves at ionospheric heights," Can. J. Physics, 38, 1441-1481.

Houghton, J. T., 1978, "The stratosphere and mesosphere," Quart. J. Roy. Met. Soc., 104, 1-29.

Kent, G. S., P. Sandland and R. W. H. Wright, 1971, "A second generation laser radar," J. Appl. lMeteor., 10, 443-452.

Kneizys, F. X., E. P. Shettle, W. O. Gallery, J. H. Chetwynd, Jr., L. W. Abreau, J. E. A. Selby, R. W. Feen, and R. A. McClatchey, 1980, "Atmospheric Transmittance/Radiance: Computer Code LOWTRAN 5 AFGL-TR-80-0067, Air Force Geophysics Laboratory, Hanscom AFB, MA.

Lindzen, R. S., 1981, "Turbulence and stress due to gravity waves and tidal breakdown," J. Geophys. Res., 86, 9707-9714.

McCormick, M. P., 1986, "SAGE Aerosol Measurements," NASA Reference Publication 1149, NASA Scientific and Technical Information Branch, Washington, DC.

Patterson, E. M. and J. B. Gillespie, 1987, "Development of a model for UV propagation," Paper presented at EOSAEL Conference, Las Cruces, NM, December 1-3.

Post, M. J., 1984, "Aerosol backscattering profiles at CO_2 wavelengths: the NOAA data base," App. Opt., 23, 2507-2509.

Schmidt, E., 1988, "High altitude effects on spectral measurements," Paper presented at 1988 SPIE Technical Symposium on Optics, Electro-Optics and Sensors, April 4-8, Orlando, FL.

Uchino, O., M. Maeda, and M. Hirono, 1979, "Applications of excimer lasers to laser-radar observations of the upper atmosphere," IEEE J. Quantum Elec., QE15, 1094-1107.

III. LIDAR Performance Requirements

The energy received from an element of range located in the interval (R, R+ΔR) by a LIDAR is

$$E(\lambda,R) = E_L K(\lambda) k_A k_T \frac{A}{R^2} \beta(\lambda_L,\lambda,R) \frac{cT_d}{2}$$

where E_L = laser energy/pulse at wavelength λ_L

$K(\lambda)$ = receiver spectral transmission factor at wavelength

k_A = atmospheric transmission at wavelength λ_L and

k_T = transmitter efficiency and geometric form factors which includes overlap of the laser irradiation area with receiver field of view

A = area of receiver mirror

R = range

$\beta(\lambda_L,\lambda,R)$ = volume backscattering coefficient

T_d = response time of the detector.

c = speed of light

The range resolution is limited to $c(T_d + T_L)/2$ where T_L is the laser pulse width. It is assumed that T_d and T_L are both much less than 2R/c.

A. Elastic Scattering LIDAR

In this system the transmitter and receiver are set at the same wavelength and the number of received photons per time are recorded. From these data and the parameters of the LIDAR system, the elastic backscattering coefficients can be calculated. The backscattering coefficient is a sum of products of two terms in this case that can be written as

$$\beta(\lambda_L R) = \sum_i N_i(R)\sigma_i(\lambda)$$

where $N_i(R)$ = number density of species i

and $\sigma_i(\lambda)$ = backscattering cross section for species i.

The most straightforward use of the backscattering measurements is to use the fact that an abrupt change in the density of one of the scattering species will cause the backscattering coefficient to give a discontinuity in the returned energy. In this way the structural features of clouds such as ceiling, base height and the location of other discontinuities can be measured. However, determining the composition of the clouds by LIDAR measurements is not straightforward because of the complexity of the scattering processes within the cloud.

A fairly simple addition to the LIDAR system does allow more characterization of the cloud composition. This is based on the fact that scattering by nonspherical particles does not preserve the polarization of the incident radiation. So, by adding polarization analyzers in front of the receiver, the ratio of the amount of received power polarized parallel to that polarized perpendicular, the depolarization ratio, can be measured. These measurements can be used to give some indication of the distribution of ice and water within the cloud.

Another kind of measurement with this kind of system is to obtain the density of a particular scattering species, i.e., nitrogen. To obtain this from the measured backscattering coefficients, the various products in the expression above must be determined. Usually, this is done by assuming that the backscattering coefficients are either due to Rayleigh scattering from molecules or Mie scattering from larger size species. The molecular Raleigh scattering depends on the wavelength as λ^{-4} whereas the Mie has another wavelength dependence. Thus, if the backscattering coefficients are measured at two wavelengths, the different wavelength dependence can be used to separate the Rayleigh and Mie contributions. The nitrogen density then can be obtained from the Rayleigh part by using the well known backscattering cross section and, assuming that nitrogen molecules are the major contribution to the scattering. (See Section II.)

The Mie scattering coefficients can be used to obtain an integrated aeroarticulate density for all species large enough to give Mie scattering if a means of calibrating the measured back-

scattering coefficients to known integrated densities is available. The calibration can be done by using a density measured by another method, a balloon-borne counter for example, at a known altitude or by using an appropriate model to calculate a density for calibration. Thus, the atmospheric parameters that can be measured with an elastic scattering type LIDAR are cloud structural features, some indication of the relative water-ice composition, molecular density of air from which temperature and pressure can be calculated assuming the ideal gas law, and aero-articulate densities.

Figures 4 through 6 show the results of simulations for the number elastically scattered photons received per second for various instrumental conditions.

B. DIAL LIDAR

In the general LIDAR equation above we assume two lasers with wavelengths λ and $\lambda' = \lambda + \delta\lambda$ where $\delta\lambda$ is usually a few tenths of λ. If we assume that the power of the two lasers is the same and that

$$K(\lambda) = K(\lambda')$$

$$k_T(\lambda) = k_t(\lambda')$$

$$\beta(\lambda) = \beta(\lambda')$$

then the equations for $E(\lambda,R)$ and $E(\lambda',R)$ can be combined to give the number density of an absorbing species

$$N(R) = \frac{1}{2\sigma_A(\lambda,\lambda')} \frac{d}{dR} \ln \frac{E(\lambda',R)}{E(\lambda,R)}$$

where the differential absorption cross section, $\sigma_A(\lambda,\lambda') = \sigma_A(\lambda) - \sigma_A(\lambda')$.

The analysis above is the basis for a differential absorption LIDAR or DIAL that uses backscattering from the atmosphere to provide the returns in place of a distant retro-reflector. In practice one of the wavelengths is chosen to correspond to a molecular absorption and the other to a value

just off of the absorption. This technique then is species specific and, in principle, is independent of the system parameters that are required for data analyses in the elastic system. Thus, reliable densities can be obtained without resorting to other experimental data or models for calibration. It is also possible to measure the temperature at a distance R using the fact that the absorption linewidth and hence the differential absorption depends on temperature. However, a detailed analysis shows that a third wavelength is needed to avoid an independent temperature measurement for calibration.

The range for DIAL is considerably less than with elastic LIDAR because of the absorption that is the basis of the technique. Nevertheless, the large receiver area of the MEGALIDAR makes this an attractive technique for measuring small concentrations of certain species. Of particular interest is the possibility of using the absorptions at 720nm, 930-960nm and 10.26 micrometers for DIAL measurements of water vapor concentrations. A specific application of DIAL to measurements of ozone concentrations is discussed in Section II.

C. Raman LIDAR

Raman LIDAR is also a two wavelength LIDAR that transmits a wavelength, λ, but receives a slightly different wavelength, $\lambda+\delta\lambda$. The received wavelength is shifted by Raman scattering which is a process by which the scattering molecule adds or subtracts some of its internal vibrational and rotational energy to the scattered radiation and thus changes the scattered wavelength. Thus Raman LIDAR is molecule specific and since Raman scattering cross sections for molecules of interest in atmospheric studies are well known, densities can be obtained from the measured backscattering coefficients. As in the case of elastic LIDAR, the transformation from backscattering coefficient to absolute density requires precise values of the system parameters given in the LIDAR equation or a density measurement by another method for calibration of the LIDAR data.

It is also possible to obtain temperature values from Raman

LIDAR measurements because the size of the Raman shift depends on the distribution of the molecules among the possible rotational states and this distribution affects the size of the Raman shift for a given molecule. Detailed analysis shows that a differential technique using two wavelengths eliminates most of the uncertainties in the temperature measurements. Simulations of Raman LIDAR from nitrogen using the MEGALIDAR are given in Section II.

On comparing the three LIDAR techniques discussed so far in terms of the scattering, we can describe the first as a completely elastic collision between an incident LIDAR photon and a molecule, the DIAL uses a completely inelastic collision in an absorption of a photon by a molecule, and finally the Raman LIDAR uses an inelastic collision between a LIDAR photon and a molecule.

There are other important distinctions between the DIAL and Raman LIDAR methods. In the DIAL method we choose the incident wavelengths to be on and just off an absorption band of the molecule of interest which can be in any part of the spectrum where there is good atmospheric transmission and a convenient laser. Also the DIAL approach depends on the fact that the absorption cross section is 10^8 to 10^{15} larger than the Rayleigh scattering cross section at the same wavelength and thus can be sensitive to very small concentrations of absorbing species, but this also can lead to shortened ranges. Lastly, DIAL LIDAR depends on backscattering from atmospheric molecules for returns and thus is restricted to regions where there is a high enough nitrogen density to provide the necessary returns. On the other hand, the Raman scattering cross section depends on the incident radiation frequency to the fourth power so we must choose as high a frequency or correspondingly as short a wavelength as is compatible with atmospheric transmission and laser availability for effective Raman LIDAR. The amount of the shift of the scattered wavelength depends on the molecule so it is species specific, but we are not free to choose the amount of shift once the molecule is chosen and it is usually smaller than the shifts

used in DIAL. Further, the Raman scattering cross section is about 10^4 smaller than the Rayleigh cross section at the same wavelength so the minimum detectable concentrations are smaller for Raman than DIAL, but there is no sharp range cutoff as there can be in DIAL.

There are some important comparisons of the experimental systems for Raman and DIAL also. Both require narrow, stable spectral output in addition to the usual LIDAR requirement of short pulses with stable pulse to pulse power. DIAL systems can require two laser systems that must have their pulses synchronized so that there is as short a period as possible between the pulses from each laser so that the possibility of errors from changing atmospheric conditions between on and off absorption is minimized. In addition, the output wavelength must be controlled and known to at least a few picometers in order to know what part of the absorption line is probed. Raman LIDAR requires only one laser since the shifting is done by the scatter. Both require careful control of the receiver spectral line width because the shift from the transmitter to receiver wavelength is small with the Raman almost always the smaller. So, although, the Raman requires a less complicated transmitter than DIAL, it requires more apparatus to meet the requirement that negligible transmitter light reach the detector since one wants to record the Raman scattered, not the elastic Rayleigh scatter light.

The main point of this comparison is to show that, although the DIAL and Raman LIDAR measure the same atmospheric parameters and thus appear to be redundant, in fact, each has advantages over the other in certain situations. Thus, a well equipped LIDAR facility would have access to both types.

D. Fluorescence LIDAR

A fluorescence LIDAR uses the fact that radiation that is absorbed by an atom or molecule excites it to a higher energy state that is unstable so that after a finite time radiation is emitted as the atom or molecule returns to the initial state. In atoms the emitted energy is the same wavelength as the absorbed,

but in molecules the wavelength is usually shifted to larger values. The LIDAR equation is adapted to this process by including the absorption in the atmospheric transmission factor and changing the backscattering coefficient to a product of the density of the fluorescent species and the differential fluorescent cross section which is of the order of the absorption cross section. Since the absorption cross section is many orders of magnitude larger than the Rayleigh scattering cross section, the self-absorption and collision quenching at normal tropospheric density leads to such a low transmittance that fluorescence LIDAR is of limited use in the troposphere even for minor constituents.

However, the regions of low density sodium and other atoms in the stratosphere are well suited for probing with this LIDAR technique. Because of the low density, self-absorption is not an insurmountable problem and the large absorption cross section allows LIDARs with modest capability to gather data around 100km. Measurement of the returns can be used to get relative density distributions of the atoms since the cross sections are well known. Distributions of the absolute density require precise knowledge of the LIDAR parameters or a calibration from another type of measurement. More involved measurements yield data that can be used to get the temperature distribution in this region also.

This kind of LIDAR puts some stringent requirements on the stability of the transmitter laser because of the use of an atomic absorption line which is usually a few picometers wide. Thus, in order that the transmitter be tuned to the absorption wavelength, it must have a spectral bandwidth of less than a picometer and must be stable to about one picometer. If temperature data are to be obtained, the bandwidth must be narrowed to a few tenths of a picometer because the actual shape of the absorption lines must be probed by the transmitter. In most cases a Fabry Perot interferometer is used to get the narrow bandwidth for the transmitter. Fortunately, a power of a few tens of milliwatts is enough to obtain data at 100km so dye lasers can be

used to get the required wavelength and stability.

E. CO_2 Coherent LIDAR

In the discussion above the emphasis has been on the atmospheric parameters that can be measured by the various kinds of LIDAR systems and on the distinguishing features of the systems that follow from the characteristics of the interaction of the radiation with the atmosphere. In this section the emphasis is on the features of an experimental system that are quite different from those above.

The systems that have been discussed so far all use a method of signal detection that yields an output signal that is proportional to the amplitude of the return energy, $E(\lambda,R)$. It is possible to also recover the phase of the returned energy with respect to the transmitted energy if a coherent detection system is used. In a coherent detection system a portion of the transmitted energy is mixed (heterodyned) with the returned signal and the difference signal is detected by various schemes. The choice of a detector scheme is determined by whether one actually obtains and measures the phase or only uses the fact that the phases of the return and the reference are well correlated in the mixed signal so that a precise frequency difference can be measured as in atmospheric Doppler LIDAR. Since velocity information is very important in atmospheric studies, the latter scheme is the one used exclusively in LIDAR and is the one that will be considered here.

In a Doppler LIDAR or laser Doppler velocimeter, the transmitted radiation is scattered by particles that are carried along by the moving volume of atmosphere at the velocity of the volume. Hence, the scattering imparts a Doppler shift to the return that is given by $f = 2V_r/\lambda$

where f = Doppler shift
V_r = radial velocity of the atmospheric volume
λ = transmitted wavelength.

It must be emphasized that only the component of the velocity parallel to the transmitted radiation (the radial component) contributes to the Doppler shift. Thus, it is the frequency of the returned energy compared to that of the transmitted energy that contains the velocity information. It is thus crucial for accurate data that the transmitter laser have high frequency stability and that the phase of the returns have a high correlation with the transmitted energy. At present, CO_2 lasers have the frequency stability and hence the necessary coherence length as well as high power to be used in high quality Doppler LIDARs.

There are two configurations that have been used with CO_2 lasers in Doppler LIDAR systems. One, the homodyne scheme, uses one laser that serves as transmitter and local oscillator. The optical arrangement is made so that a small amount of power from the transmitter is coupled to the mixer. With the homodyne it is convenient to provide zero frequency offset at the mixer so that the sign of the Doppler shift can be measured and hence the radial velocity direction. In the other arrangement, the heterodyne scheme, the local oscillator energy is supplied by another laser that also supplies a small amount of energy to injection lock the high power laser to insure high phase correlation. Usually the transmitter is frequency locked at several tens of MHz from the local oscillator to provide an IF that is the difference between the two frequencies. Both systems can be pulsed to obtain range information although the stabilizing systems become more complicated. Also, the two systems can be made coaxial to simplify the optics because the polarization of the backscattered beam is rotated 180 degrees from the incident beam so that the transmitted beam can be made right circularly polarized and kept separate from the received beam which will be left circularly polarized. The heterodyne system is more complicated and expensive, but is more versatile because it can be used for a very sensitive heterodyne detection LIDAR with a high power transmitter in addition to a Doppler LIDAR.

F. Turbulence Effects on Coherent Detection

Atmospheric turbulence will place limits on the size of the receiver to be used in heterodyne reception since coherent detection requires that the backscattered radiation be in phase over the entire system pupil. Based on discussions in Hufnagel (1978) and in Shapiro, et al (1981), the limiting maximum signal-to-noise ratio that can be achieved is reached when the diameter of the system's entrance pupil exceeds the coherence diameter. The pupil diameter, which for the case of the proposed 100-inch system will be the aperture of the telescope, must be less than or equal to the coherence diameter r_o. Values of r_o can be calculated for different wavelengths, based on an assumed turbulence profile.

The coherence diameter r_o is defined according to the equation

$$r_o = \left[\frac{D_w(r)}{6.884\ r^{5/3}} \right]^{-3/5}$$

where $D_w(r)$ is the wave structure function and r is a separation distance measured in a plane perpendicular to the average direction of propagation (Hufnagel, 1978).

The wave structure function is defined according to the equation

$$D_w = 2.914\ k^2\ r^{5/3} \int_o^L C_n^2(z)\ \left(1 - \frac{z}{L}\right)^{5/3}\ dz$$

for the spherical wave propagation that is appropriate to the proposed LIDAR system. L is the propagation path length; z is the distance along the propagation path measured from the receiver; and C_n^2 is the turbulence strength parameter. The equation is weighted so that turbulence close to the receiver is more important than turbulence near the target.

For vertical paths in the daytime, the turbulence profile follows an approximate relation of the form

$$C_n^2(z) = C_n^2(z_o)z^{-4/3}$$

with z in meters. C_n^2 can be approximated as 1.5×10^{-13} $m^{2/3}$ at z_o = 1 m. At night, the turbulence strength at 1 m is much less than in the daytime, but falls off more slowly with height.

We have used the turbulence profile described above to calculate the coherence length to be expected for a vertically pointing system, assuming a return from z = 20 km. These calculations indicate that the coherence length for the 10-micrometer laser wavelength will be significantly larger than the approximately 2.5-m aperture of the telescope and that the use of the telescope as a receiver for 10-micrometer radiation will not be limited by atmospheric turbulence. Because of the decrease in coherence length with decreasing wavelength, coherent detection is not appropriate for shorter wavelengths (such as the 1.06 micrometer, Nd:YAG wavelength).

References

Hufnagel, Jr., F., 1978, "Propagation through atmospheric turbulence," Chapter 6 of IR Handbook, ed. by W. L. Wolfe and T. T. Zissis, IRIA, Ann Arbor, MI.

Shapiro, J. H., B. A. Capron, and R. C. Harney, 1981, "Imaging and target detection with a heterodyne-reception optical radar," Appl. Opt., 20, 3292-3313.

IV. Characterization of Available Instruments

In this section the characteristic of the principal components of the LIDAR systems that were described in Section III will be discussed. The discussion will be restricted to characteristics that are relevant to LIDAR and to components that are presently available commercially.

A. Transmitters

The ideal LIDAR transmitter laser, as seen from the discussions in Section III, should have at least the following properties: (1) high energy per pulse for long maximum range, (2) a short pulse that has high time stability from pulse to pulse for high range resolution, (3) high pulse repetition rate for rapid data gathering, (4) continuously tunable to the wavelength of the phenomenon to be studied, (5) small deviation from the chosen wavelength for reproducible data, (6) narrow, stable spectral bandwidth for accurate probing of absorption lines and Raman scattering, and (7) narrow, well defined output beam divergence for low light scattering, ease of optical manipulation and high spatial resolution.

Unfortunately, there is no one laser that will meet all these criteria, especially number 4 since one laser that covers all the wavelengths that are of interest for remote sensing of the atmosphere is not available. Further, satisfying one of the criteria precludes meeting another with lasers available today. For example, a laser with high pulse energy compromises the requirements on spectral stability. Thus, we must balance the requirements in making the choice of lasers and a single laser is a compromise of some of the ideal requirements. This gives another reason to add to those in Section III for a multilaser approach to the MEGALIDAR facility.

Table 3 lists the types of lasers that are commercially available that have been used in successful LIDAR systems. Also included are typical wavelengths of the output, the energy per pulse, E, in Joules, pulse rate, P, in Hz, a typical pulse width, T_L, in ns and a commercial supplier. A somewhat arbitrary cutoff

TABLE 3. Characteristics of Lasers for LIDAR

LASERS		F(J)		P(Hz)	T_L(ns)	MANUFACTURER MODEL NO.
(μm)	Type	TEM	MM			
0.694	Ruby	0.5		1/3	25	Quantel RB 18A
1.061	Nd:YAG	0.61		30	10	Quantel 581-30
0.530		0.22		30	9	Quantel 581-30 SHG
0.354		0.08		30	8	Quantel 581-30 THG
0.266		0.03		30	7	Quantel 581-30 FHG
0.308	XeCl Excimer		0.325	0-125	20	Questek Inc. 2660
0.35	XeF Excimer		0.2	0-200	11	Questek Inc. 2460
0.73-0.78	Alexandrite $Cr:BeAl_2O_4$		0.2	10	100	Appolo Lasers
9-12	CO_2	0.17	0.3	0-150	130	Laser Science Inc. PRF 150
3.5-4	DF	0.2	0.7	1-2	500	Lumonics TEA-200-2
2.6-2.8	H_2	0.5	1	3	100	Lumonics TE-270
1.32	I_2		1	<1	15	Quantum Elec. Inst. IL200
0.45-0.7	Dye		Var.	30	10	Quantel
0.6-40	Semiconductor		Var.	Var.	Var.	Spectra Physics

in energy per pulse was used in making the list, but it is based on the assumption that the MEGALIDAR will be used primarily for middle and upper atmospheric research and thus will require energies above this level. Dye lasers, in principle, cover a wide range of wavelength in the visible and can produce radiation in the near infrared by various means, such as Raman shifting, but the output energy is not uniform. Semiconductor laser diodes are sources of radiation in the infrared that have recently become available with pulse energies above 10 mW. However, they have the distinct disadvantage of having a very large beam divergence.

B. Detectors

The ideal detector for a LIDAR system should have at least the following characteristics: (1) a large enough area that it can be easily and efficiently coupled to the received light beam, (2) a 100-percent efficiency for converting photons into electrons, i.e., it produces one electron for one signal photon, (3) it does not produce any random fluctuations of the electron current (noise) that it adds to the signal, (4) it has a bandwidth that allows for reproduction of the return pulses with high fidelity, and (5) its electrical characteristics are such that when connected to the following electronics the performance of the system including the detector is not degraded.

Even though we cannot get a real detector that meets all these specifications, we should use them as a minimum set of standards against which any real detector is judged. The list emphasizes that there is not just one figure of merit that can be used to select detectors and that it is risky to extrapolate the evaluation of a particular detector for a certain application to its performance in another application. For example, it does not follow that a detector, which provides an acceptable performance for a system that uses a low modulation frequency, will give the same performance in a system that uses pulses of nanosecond duration.

The performance of a detector can be evaluated by estimating

the signal-to-noise ratio (SNR), the noise equivalent power (NEP) which is the amount of received power required to give a SNR of unity or the minimum detectable energy, the energy required for a specified SNR. The two most common ways of calculating the SNR is to use the ratio of the signal current in the detector to the root mean square of the total noise current or to use the ratio of the signal power to the average noise power. The latter amounts to the ratio of the square of the signal current to the mean square of the noise current.

These definitions can be expressed as follows:

$$(SNR)_C = i_S / \sqrt{\overline{i_N^2}} \text{ or } (SNR)_P = i_S^2 / \overline{i_N^2}.$$

$$i_S = \frac{CGe\eta\overline{P_S}}{h\nu} = \frac{GCe\eta E_S}{h\ T_g},$$

where

η = the detector quantum efficiency,

G = electron number gain of PMT or avalanche photodiode,

C = collection efficiency of first PMT dynode,

T_g = the observation time or the sampling time,

$\overline{P_S}$ = the average power of the return pulse,

E_S = the peak energy of the return pulse, and

$$\overline{i_N^2} = \frac{e^2G^2C(n - \bar{n})^2}{T_g^2}.$$

Assuming Poisson statistics for the noise, the mean square fluctuation of the number of noise electrons, $(n - n)^2$ is equal to n when averaged over many independent observation times. Thus,

$$\overline{i_N^2} = \frac{e^2G^2C\bar{n}}{T_g^2} \quad \text{and} \quad \sqrt{\overline{i_N^2}} = \frac{eG\sqrt{C\ \bar{n}}}{T_g}.$$

The accuracy of the estimate of the SNR for a particular detector then depends on the correct identification and

representation of the noise sources. These noise sources usually come from the following mechanisms: statistical fluctuations of the return radiation or photon quantum noise, statistical fluctuations of the background radiations, thermal generation of current carriers in the detector with no radiation on it, and thermal energy of the carriers or Johnson noise.

For example, these noise mechanisms can be represented by the following expressions for the mean square of the noise fluctuations:

$$\bar{n}_s = \frac{\eta E_s}{h\nu} \quad \text{signal photon noise}$$

$$\bar{n}_b = \frac{\eta E_b}{h\nu} \quad \text{background photon noise}$$

$$\bar{n}_d = \frac{i_d T_g}{e} \quad \text{dark current noise}$$

$$\bar{n}_R = \frac{2kT_N T_g}{e^2 R} \quad \text{Johnson noise from an equivalent load resistor for the detector connected to a preamplifier of noise figure F.}$$

$T_N = T_R + (F-1)T_{300}$. T_R is the temperature of the equivalent load resistor.

Putting these into the expression for the $(SNR)_c$ gives

$$(SNR)_c = \frac{E_s/E^{1/2}}{\left[E_s + E_b + \frac{E}{2eB}\,(Ci_d + i_J)\right]^{1/2}}$$

where $E = h\nu/C\eta$, $i_J = \frac{2\ k\ T_N}{eCG^2R}$ and $B = \frac{1}{2T_g}$ is the bandwidth of the system.

This expression can be used to estimate the $(SNR)_c$ for detectors that have electron multiplication such as PMTs and avalanche photodiodes and other detectors such as infrared photodiodes that have C and G equal to unity and are connected to

a preamplifier with a noise figure, F, with the equivalent load resistor at T_R. In the case of the detectors with high G, the i_J is usually negligible compared to other noise terms.

Even though the general case is rather complicated, there are several limiting cases that give some useful bounds to the general cases. If all sources of noise in the detector and the background are eliminated or are small compared to the signal energy we still have the quantum noise from the signal photons.

So if, for whatever reason,

$$E_s >> E_b + \frac{ECi_d}{2eB} ,$$

then the above expression gives for $(SNR)_c = 1$,

$$E_s = \frac{h\nu}{\eta C} .$$

Thus, the number of photons/second received during one observation time is

$$\text{photons/s} = E_s/h\nu T_g = \frac{2B}{\eta C}$$

which is the minimum that can be achieved by any detection system.

It is also useful to consider the background limited case where the quantum noise from the background radiation is the predominant term. In this case,

$$E_b >> E_s + \frac{E}{2eB} (Ci_d + i_J)$$

$$\text{so} \quad (SNR)_c = \frac{E_s/E^{1/2}}{E_b{}^{1/2}}$$

and for $(SNR)_c = 1$

$$E_s = \left[\frac{S_b(\lambda)\ \Omega_o\ A\ K\ T_g\ h\nu}{\eta C}\right]^{1/2} .$$

$$\text{The photons/s} = \frac{E_s}{h\nu T_g} = \left[\frac{S_b(\lambda)\ \Omega\ A\ K}{\eta\ C\ T_g\ h\gamma}\right]^{1/2}$$

where S_b = the spectral radiance of the sky background in W $cm^{-2}Sr^{-1}\mu m^{-1}$ and Ω = the acceptance solid angle of the receiver.

Table 4 gives the spectral range and compares the NEP for detectors that are most commonly used in LIDAR systems. The NEP for the short wavelength PMT was calculated at a wavelength of The NEP for the long wavelength PMT was calculated using a quantum efficiency of 0.3 percent and a daylight background radiance of $5x10^{-4}$ W $cm^{-2}Sr^{-1}\mu m^{-1}$. The values for the other detectors are typical values given by manufacturers for dark current limited operation.

TABLE 4. Characteristics of Detectors for LIDAR

DETECTOR	TYPE	SPECTRAL RANGE (μm)	NEP(W/Hz$^{1/2}$)	TEMP(K)
PMT	Alkali Photocathode	0.25 - 0.65	$2x10^{-14}$	273
PMT	S-1	1.06	$1X10^{-12}$	273
APD	Si	1.06	$1x10^{-13}$	300
PD	Ge	0.9 - 1.7	$2x10^{-12}$	300
PD	InSb	2 - 5	$1x10^{-12}$	77
PD	HgCdTe	8 - 12	$5x10^{-12}$	77
PC	HgCdTe	2 - 15	$1x10^{-11}$	77

C. Maximum Range for MEGALIDAR with Rayleigh Scattering

By using the signal quantum noise limit, we can estimate the maximum range for the MEGALIDAR using Rayleigh backscattering.

Equating the minimum number of photons/sec = $\frac{E_s}{h\nu T_g}$ and using

the basic LIDAR equation, we get

$$\left(\frac{dn_p}{dt}\right)_{min} = \frac{E_L k_t k_A^2 \beta A K \lambda}{2R^2 h} = \frac{1}{\eta T_g} = \frac{c}{\eta 2\Delta Z}$$

where ΔZ is the increment of range sampled during T_g. Solving for β gives

$$\beta = \frac{4 h C R^2}{E k_t k_A^2 \pi r^2 K \eta \lambda \Delta Z} \quad m^{-1}sr^{-1}$$

For E = 0.5J, K = k_t = 1 and 2r = 2.54 m

$$\beta = 7.8\text{x}10^{-26} \frac{R^2}{k_A^2 \lambda \eta \Delta Z}$$

Using λ = 0.55 μm k_A = 0.72 η = 0.15 ΔZ = 1 Km or

λ = 1.06 μm k_A = 0.86 η = 0.03 ΔZ = 1 Km gives

$\beta(0.55) = 1.84\text{x}10^{-21} R^2$ or $\beta(1.06) = 3.33\text{x}10^{-21} R^2$.

The minimum β that can be observed at a range R can be calculated from the above. Several values are given in the table below.

$\beta(1.06)$ $m^{-1}sr^{-1}$	R m	$\beta(0.55)$ $m^{-1}sr^{-1}$	R m
$0.85\text{x}10^{-11}$	$5.0\text{x}10^{4}$	$4.6\text{x}10^{-12}$	$5.0\text{x}10^{4}$
$1.0\ \text{x}10^{-11}$	$5.5\text{x}10^{4}$	$0.6\text{x}10^{-12}$	$6.0\text{x}10^{4}$
$1.2\ \text{x}10^{-11}$	$6.0\text{x}10^{4}$	$0.9\text{x}10^{-11}$	$7.0\text{x}10^{4}$
$1.4\ \text{x}10^{-11}$	$6.5\text{x}10^{4}$	$1.15\text{x}10^{-11}$	$8.0\text{x}10^{4}$
		$1.45\text{x}10^{-11}$	$9.0\text{x}10^{4}$

Using the values of $\beta_{Ray}(1.06)$ given on the graph in Figure 1 a match of the values of $\beta(1.06)$ above, β_{Ray}, and R occurs between

R = 60 and 65 Km.

The values of $\beta_{Ray}(1.06)$ from Figure 1 can be scaled by $(1.06/0.55)^4$ to find $\beta_{Ray}(0.55)$. The same matching procedure gives the maximum range for 0.55 μm radiation at 80 to 90 Km.

D. Spectral Filtering and Beam Chopping

In the expression for the minimum detected energy in the background quantum noise limited case, we have the spectral bandwidth function at one's disposal to increase the sensitivity of the system. This is usually done with filters with narrow spectral bandpass or, in extreme cases, with prism monochromators or Fabry Perot interferometers.

The effect of the spectral band pass, $\Delta\lambda$, can be quantified using the spectral rejection ratio which is established for each kind of LIDAR system. For example, an elastic LIDAR operating in the daylight will operate in the sky background limited SNR case only if the background from backscattered radiation from the laser in the wavelength range around the central wavelength is limited in some way. Thus,

$$\eta\ E_L^{\,b}\ (\lambda_L) \ll E_b\ (\lambda) \text{ or}$$

$$\eta\ E_L\ K(\lambda_L)\ k_A^{\,2}\ \frac{A_o}{R^2}\ \beta(\lambda_L)\ \frac{cT_g}{2} \ll S_b\ A_o\ \Omega\ T_g\ f(\lambda)\Delta\lambda$$

so the rejection ratio must satisfy the inequality,

$$\frac{K(\lambda_L)}{f(\lambda)} \ll \frac{2\ S_b\ \Omega\ R^2\Delta\lambda}{\eta\ E_L\ k_A^{\,2}\ \beta(\lambda_L)c}$$

where the spectral bandwidth function is written K( ) = f( ) .

If we used the following parameters for the MEGALIDAR,

$$S_b = 7\text{x}10^{-3}\ \text{W cm}^{-2}\ \text{Sr}^{-1}\ \mu\text{m}^{-1},$$

$$\Omega = (2.9\text{x}10^{-3})^2,$$

$$A = \left(\frac{254}{2}\right)^2 \pi\ \text{cm},$$

$$\Delta\lambda = 10^{-2}\ \mu\text{m},$$

$R = 80x10^3$ m ,

$\lambda_L = 0.53$,

$\eta = 0.15$,

$k_A = 0.72$,

$E_L = 0.5J$,

$\beta = 1.2x10^{-11}$ m^{-1} Sr^{-1} ,

the inequality becomes $K(\ _L)/f(\ ) << 1.5x10^8$ which means at the range of 80 km the backscattering coefficient is so small that backscattering from wavelengths around the central wavelength will not dominate the sky background. Thus, we only must limit the sky background.

For Raman LIDAR the extinction ratio is determined by the condition that the backscattered radiation from the laser be less than the Raman backscatter signal. Thus,

$$\eta\ E_L\ (\lambda_L) << E_R(\lambda)$$

which leads to

$$K(\lambda_L)/f(\lambda) << \frac{\sigma_R\ N}{4\pi\ \beta(\lambda_L)\ \eta}$$

where σ_R is the Raman scattering cross section, N is the number density of the scattering species and it is assumed that the atmospheric transmission coefficient is the same for the incident and scattered radiation.

If the MEGALIDAR is used for Raman LIDAR to measure nitrogen number densities at 30 km using 0.53 micron radiation from a doubled Nd:YAG laser, then the rejection ratio would have to be less than $7x10^{-6}$ which would require a monochromator or Fabry-Perot interferometer. It should be noted that the Raman rejection ratio doesn't depend on the parameters of the LIDAR instrument, but only on the characteristics of the observed species.

In a real case we must limit the transmitter laser scattering within the system so that the assumptions in the above

calculation of the rejection ratios are met. That is, that the only unwanted returns are coming from scattering outside the system where it cannot be controlled. These conditions require great care in the optical design, and may include filtering or chopping the transmitter beam. Special attention will need to be paid to this for the MEGALIDAR because of the large collection area of the mirror.

Also, because of the large collection area of the MEGALIDAR mirror it will be necessary to chop the return beam for returns below about 20 km. Returns from this range will give such a large signal that the detectors will be saturated and will not recover sufficiently to give accurate data for the returns for larger ranges. So, the radiation from the lower ranges will have to be shielded from the detectors by a motor driven chopper that turns fast enough to give a sharp cutoff and is synchronized with the transmitter pulse. (See Section V.B also.)

E. Noise Reduction

There are two additional ways of increasing the sensitivity of LIDAR systems that apply in special cases. One is the use of a heterodyne detection system similar to the one described in Section III. Under the ideal conditions of a mixing ratio of one for the local oscillator and 100 percent for the quantum efficiency of the mixer, this scheme gives the minimum number of photons per second for a SNR of one as

$$\frac{2}{\eta T_g}$$

which is just twice the rate for the ideal signal quantum noise limit. In principle, the heterodyne scheme will work for any wavelength, but the required stability and frequency control for the lasers has only been achieved with the CO_2 laser to date, so this high sensitivity is restricted to LIDARs using wavelengths around 10.6 microns.

The other way of limiting the noise is the use of a photon counting technique which counts pulses from individual photons by using scalers and a multichannel analyzer to give channels for

each range sample. A discriminator amplifier is also used to discriminate against the low level noise generated by the detector. Although this method adds several pieces of equipment to the detection system, it can, when used under the right conditions give sensitivities approaching the signal quantum noise limit.

There are two important conditions for the application of photon counting methods. The detector must have a noise spectrum that can be effectively limited with the discriminator amplifier. To date the only detectors that have been successfully used are special low noise PMT's that can be cooled to about 0°C. Also the photon count rate cannot be so high that it precludes the counting of individual photons. Thus, photon counting should be used on the MEGALIDAR for the PMT detection systems and for returns coming from the longer ranges. (See Section V.B also.)

F. Data Handling

For higher return rates we must use the so called analogic method for recording the data. In this case the output of the detector is an average of many signal pulses. In the simplest data collection system, this average, which is an electronic signal, is recorded on a strip chart recorder to give a record of the return versus time or range. This scheme can be adapted to more sophisticated data recording and analysis with computers by using fast analog to digital converters that digitize the analog signal so that the data can be stored in bins according to range. The bit accuracy and conversion rate of the A/D converter must be compatible with the pulse rate and desired range resolution of the MEGALIDAR system. At present 10-bit resolution at 20 MHz is available in commercial A/D converters.

Finally, it should be noted that the accuracy of a LIDAR measurement is ultimately related to the SNR by

$$\sigma = (\mathrm{SNR})^{-1},$$

where σ is the standard deviation of the measurement fluctuations. One of the great advantages of computer data

handling that make it a necessity in sensitive LIDAR systems is the fact that data from repeated measurements over the same range values can be obtained and automatically averaged. If the successive pulses from the repeated measurements are uncorrelated, then the standard deviation of the mean obtained from n repeats is

$$\sigma_n = \frac{\sigma}{\sqrt{n}} \quad .$$

Obviously, this also assumes that the phenomenon in the observed volume that gives the measured returns and the measuring LIDAR system are not changing during the averaging time. This usually limits averaging times to the order of minutes.

V. LIDARs Classified by Optical Design

The measurements performed by the LIDAR dictate optical designs which can be grouped in categories. The most convenient and useful grouping is by field of view. Potential MEGALIDAR receiver designs can be grouped in two categories: (1) wide field systems with fields greater than 0.5 mrad, and (2) narrow field systems with fields less than 0.5 mrad. Requirements such as spectral discrimination, minimum background power, and spectral region can also be grouped according to field of view sizes.

The field of view of the receiver directly determines the transmitter characteristics. The divergence of the laser beam must be smaller than the receiver field so the beam does not spread out of the receiver field. However, the receiver field must be large enough to include the diameter of the laser beam if the beam has been expanded, plus the divergence of the expanded beam. Wide field systems may use an unexpanded beam if the beam divergence is low enough and eye safety is not a concern. A narrow field system will need moderate to high beam expansion to meet the receiver field requirements. For ultra-narrow-field receivers, such as CO_2 systems, beam expansion to the diameter of the receiver telescope is required to reduce the divergence to an acceptable level.

A. Optical Terminology

This section briefly defines some of the terms used in the following discussion.

Aperture Stop: The aperture that limits the amount of light collected by the optical system. In a Newtonian telescope, such as the MEGALIDAR, the aperture stop is the primary mirror.

Chief Ray: The ray through the center of the aperture stop.

Entrance Pupil: The image of the aperture stop as seen from the object. As the entrance pupil is an image of the aperture stop, the chief ray must pass through the center of the entrance pupil.

Exit Pupil: The final image of the aperture stop as seen from the image space of the optical system. As the exit pupil is an image of the aperture stop, the chief ray must pass through the center of the exit pupil. Aperture stop images formed inside the optical system are called intermediate pupils.

Field of View: The angle subtended by the detector or field stop as seen from the exit pupil. For a single mirror or lens with a detector at its focus, the field of view in radians is theta = arctan(d/f), where d is the detector diameter and f is the focal length of the lens or mirror. This is also the angle the chief ray makes with the optic axis at the field stop. If the field stop or detector is close to the size of the diffraction spot size, the edge of the field is ill defined. The same is true if the detector is not at the focus of the system.

Field Stop: The aperture that limits the maximum angle the chief ray can make with the optic axis of the system. The field stop lies at the image plane of the optical system and may be the detector itself. As the chief ray must pass through the center of the aperture stop, the field stop can never be the aperture stop.

B. Wide Field MEGALIDAR Receivers at Short Wavelengths

This category is comprised of systems operating in the 250-nm to 1.1-micron wavelength region. Photomultiplier tubes are used for the detectors, although avalanche photodiodes may provide better sensitivity near the red end of the region. Optical materials transmitting visible light are used throughout the system, although particular care must be used in selecting components for the UV end. Only materials such as UV grade fused silica perform acceptably, as commonly available optical glasses cut off below about 300 nm. Fluorescence of dust on the optics as well as the optical materials themselves must be considered when working with UV LIDARs. Figure 8 shows a wide field receiver which could be used for elastic scattering LIDAR.

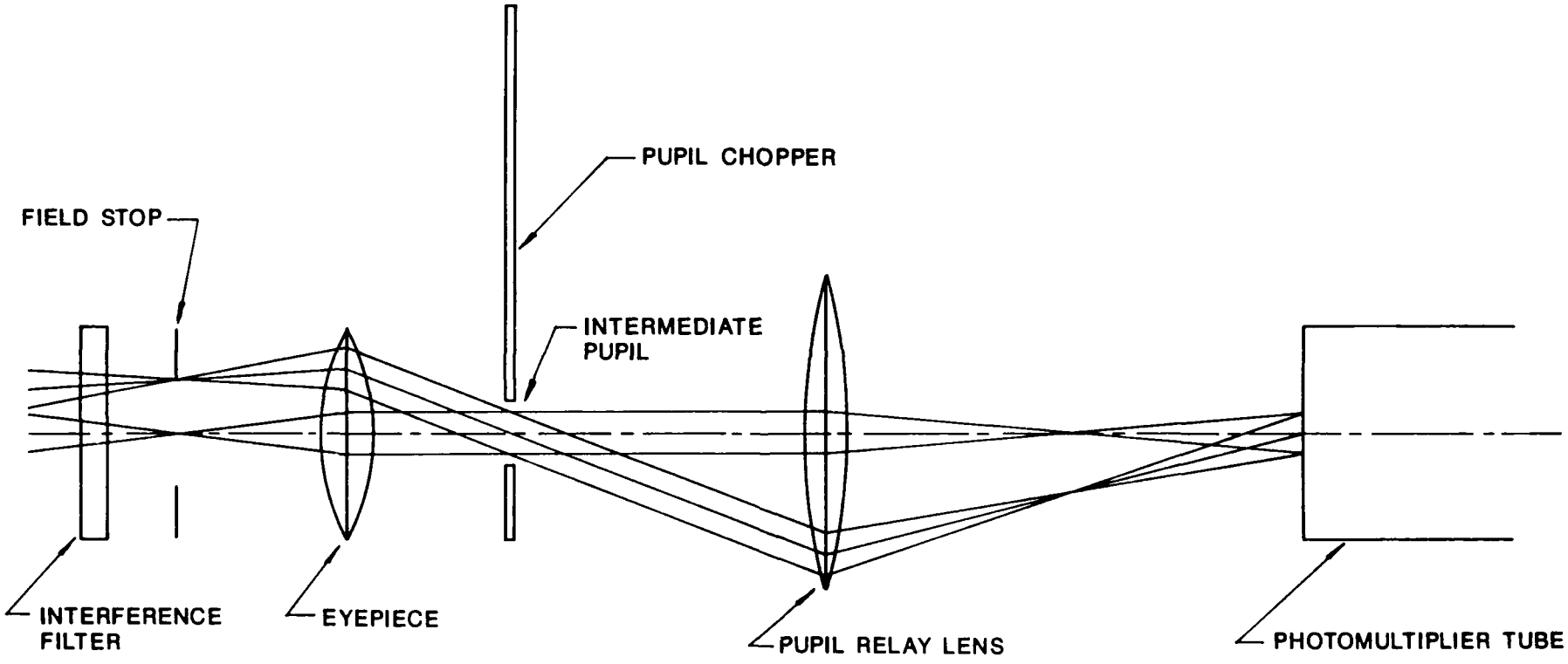

Fig. 8. Wide Field Receiver for General Use

The field of view is determined by a field stop, no more than a plate with a hole in it. The stop is placed slightly behind the infinite object distance focal plane to accommodate a slight defocus for targets above 20 km. A single lens or lens system is positioned behind the field stop with its focal point coincident with the field stop plane. This is often called the "eyepiece" from the similarity to astronomical telescopes for visual observations. Light passing through the eyepiece is collimated, or nearly so depending on the amount of defocus. The eyepiece also forms an image of the primary mirror on the other side of the lens from the field stop. This image is called the exit pupil and all light within the receiver field of view that strikes the primary mirror passes through this image. A ray through the center of the primary mirror must pass through the center of the exit pupil. The size of the exit pupil is very nearly determined by the magnification of the eyepiece/mirror system.

The exit pupil is the ideal place to position the chopper blade for blocking the near field return. As the exit pupil is an image of the primary mirror, its position is unaffected by defocus of backscattered laser light. All light collected by the system (and not blocked by the field stop) must pass through the exit pupil (and any intermediate pupil images), regardless of target distance, so the time response of the chopper blade is the same for all target distances. A chopper near the field stop would have to contend with a spot that changed size as the pulse traveled upward. Light could easily get around a field stop chopper, effectively making the chopper unblock the detector when the signal level was still too high.

If observations are restricted to altitudes above 20 km, the chopper has 130 microseconds to completely unblock the exit pupil. Assuming a 4-mm-diameter exit pupil 75 mm from the center of the chopper blade requires the blade to turn at 3900 rpm. As this arrangement will allow some near field return to slip past the blade, the chopper must turn about twice as fast. Ten thousand rpm will provide complete pupil blocking up to 12 km for a

4-mm-diameter pupil. The pupil will be completely unblocked when the laser pulse reaches 20 km. Spinning the chopper faster and/or making the pupil smaller will provide more effective blocking to higher altitudes. The laser must be synchronized with the chopper so it cannot fire unless the chopper is correctly positioned over the exit pupil.

An optical filter must be added to the system to reduce the background level or isolate the detector from the laser wavelength (See Section III.) Commonly available narrowband interference filters have tilt tolerances of 5 degrees, and bandwidths of 10 nm or less. The light cone from the 100-inch mirror converges at about 4.8 degrees half angle. The tilt tolerance allows the filter to be positioned in this converging light cone ahead of the field stop without greatly shifting the passband of the filter. The filter should be placed ahead of a telecompressor lens, as the light cone converges faster after passing through the lens. Blocking the laser wavelength may be done with a colored glass filter if the wavelength of interest is far enough away from the laser wavelength.

The light exiting the eyepiece is collimated or diverging very slowly for any object point in the field, and this initially appears to be a better position for the interference filter. Closer inspection shows that the collection of these nearly-collimated bundles for a laser spot of finite angular subtense can diverge very rapidly. For the MEGALIDAR, a 25-mm focal length eyepiece will produce a 4.2-mm-diameter exit pupil, and the light exiting this pupil will be diverging at 35 degrees for a 1-mrad divergence laser beam. An interference filter will function poorly in this position unless the laser beam is expanded to reduce its divergence.

The PMT may be placed directly behind the chopper, close enough to intercept all of the light passing through the exit pupil. As PMT's exhibit some nonuniformity across their photosensitive surface, different points in the field will have different responses from the PMT. A lens that relays the exit pupil to the surface of the PMT eliminates this problem, as the

exit pupil is stationary for all field angles. The pupil at the chopper is then known as an intermediate pupil. The exit pupil illumination does not change as the signal spot moves in the field stop, unless the signal spot is partially blocked by the field stop. The photocathode of the PMT may be approximately half covered by the exit pupil for direct detection work since most of the nonuniformities occur near the photocathode edge.

When dealing with weak signals, such as in photon counting work, as much stray light as possible should be eliminated. The field stop eliminates unwanted light from outside the field of view. A stop matching the diameter of the intermediate pupil near the chopper will help eliminate stray light from inside the field of view. This stray light can come from skylight scattered off the sides of the MEGALIDAR tube, for example. The pupil mask will prevent the scattered light from passing into the receiver as the mask only allows light reflected from the primary mirror to pass. Pupil masks may also block the image of the central obstruction to reduce stray light scattered off the support structure.

Even if the laser beam divergence is low enough to use the unexpanded beam, beam expansion may still be useful. Expansion will reduce the spot size in the field stop plane, and reduce the divergence of the light out of the intermediate pupil as well. Expansion would also be necessary if a smaller intermediate pupil at the chopper was desired as a small diameter, short focal length eyepiece cannot accommodate a large field stop diameter. Expanding the beam also allows a smaller field stop to be used, reducing the background level.

Wide field systems using low divergence lasers require little or no beam expansion to reduce the divergence further. If beam expansion is desired, refractive beam expansion telescopes that bolt onto the front of the laser can be purchased or fabricated. Expansion ratios of 5X or 10X are easily achieved, and bolting the expander to the laser makes for a mechanically rugged system. Expanding the beam also lowers the energy density on the beam steering mirror used to fold the beam up out of the

MEGALIDAR tube. The mirror coating will not degrade as rapidly from laser pulse damage, but the telescope lenses must have high quality surfaces and coatings to withstand the high pulse powers.

C. Enhancements to the Basic Wide Field Receiver

The receiver configuration shown in Figure 8 can provide moderate to high spectral resolution for observations conducted at a single wavelength. A basic receiver can be constructed in a compact, light-tight package that would bolt to the MEGALIDAR f/6 port. (See Section VI.)

The design must be augmented for observations requiring improved spectral resolution or simultaneous multiple wavelength observation. Interference filters with bandwidths of 0.15 nanometers and tilt tolerances of 1 degree are available as custom items. Spectral resolution can be further improved by placing a Fabry-Perot interferometer (FPI) in front of the basic receiver package. Bandwidths of 0.1 picometer can be obtained with these devices. In addition to the improved spectral resolution, wavelength scanning over a small range is possible with an FPI.

When selecting a narrowband interference filter the signal power, background power, and detector response must be considered. The relative magnitudes of these quantities will affect the maximum transmission and the out-of-band blocking efficiency of the filter. The filter is chosen to maximize the optical signal-to-noise ratio. For example, a filter may have 80 percent peak transmission, but may block the out-of-band background poorly in an area where the detector is particularly sensitive. Giving up a factor of two in peak transmission may increase the out-of-band blocking efficiency by two orders of magnitude, giving a comparable increase in the optical signal to noise ratio. The measurement requirements and LIDAR characteristics must be considered in detail before the appropriate filter can be chosen. (See Section IV.)

Simultaneous wavelength observations can be accommodated in the same basic receiver package. Dichroic filters can be inserted after the chopper to separate the two (or more) wave-

lengths and send them to separate detectors. Each detector may have its own wavelength selection system, ranging from colored glass filters to FPIs. These filters must be positioned after the dichroic filter, and the design of each separate leg of the system must accommodate the filter/detector combination used.

The basic receiver itself should be a modular system to enhance its versatility. All modules could bolt to a Newport 2 inches thick breadboard mounted to the side of the MEGALIDAR tube. Systems with different measurement capabilities could be constructed from a few independent modules with this approach.

An example of a modular system for LIDAR using the fundamental and doubled Nd:YAG wavelengths is shown in Figure 9. The telecentric lens forms an image of the chopper blade intermediate pupil at infinity, and a lens in each module reimages the intermediate pupil onto the detector surface. Detector modules may be positioned at any distance behind the telecentric lens, as long as the light cone from the telecentric lens does not overfill the module lens. The separation distance is made noncritical by the telecentric lens imaging the chopper blade pupil to infinity. The baseplates of each module are designed to nest together, making assembly and alignment easier.

The functions of components in the narrow field and wide field systems are shown in Figures 10 and 11. Once the diameter of the intermediate pupil is chosen, the light cone angle for the interference filter is determined by the focal length of the telecentric lens. The maximum angle remains the same for all field points as the chief ray of the system always passes normally through the interference filter. The exit pupil diameter on the detector surface may then be set by choosing the appropriate focal length for the module lens. Though the figures show single element lenses, multiple element units may be needed for the shortest focal length lenses (the eyepiece, for example). The only difference between the 0.53-micron and 1.06-micron systems shown are the interference filters and module lenses.

When assembling a system for the first time, pupil positions are easily found by opening the MEGALIDAR to the daytime sky and

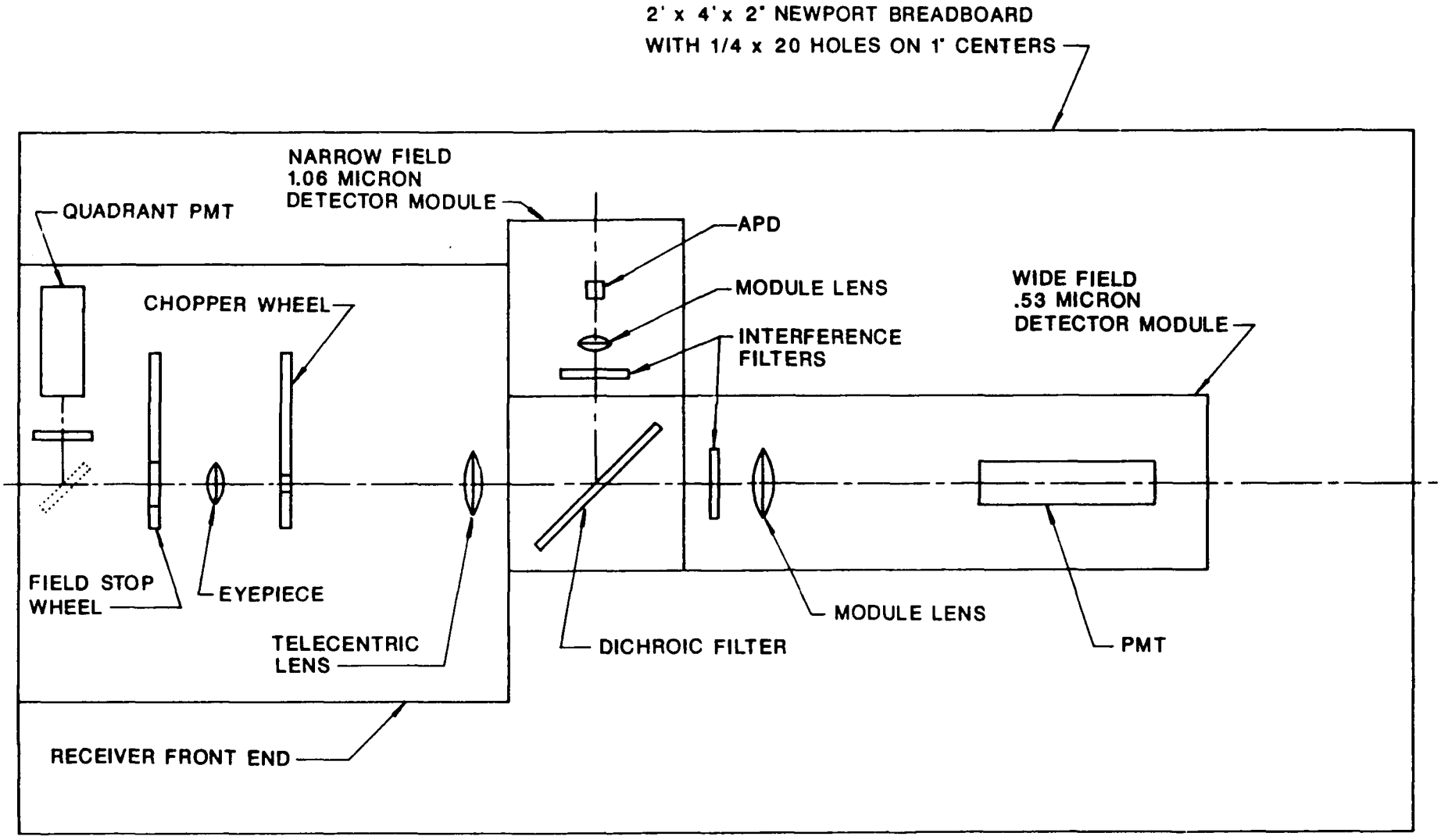

Fig. 9. Modular system for 1.06 μm/0.53 μm LIDAR.
Light Travels from Left to Right.

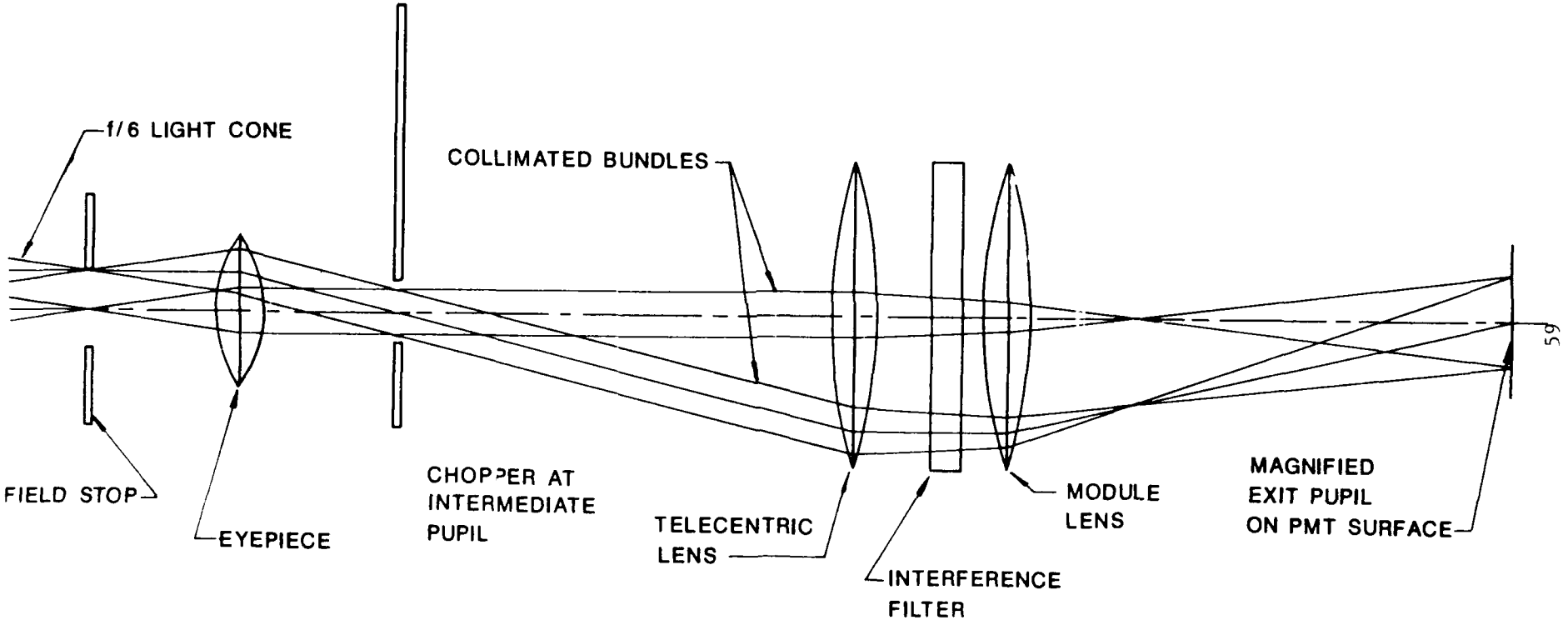

Fig. 10. 0.53 μm Leg of Dual Wavelength Receiver.
Dichroic Filter is Not Shown.

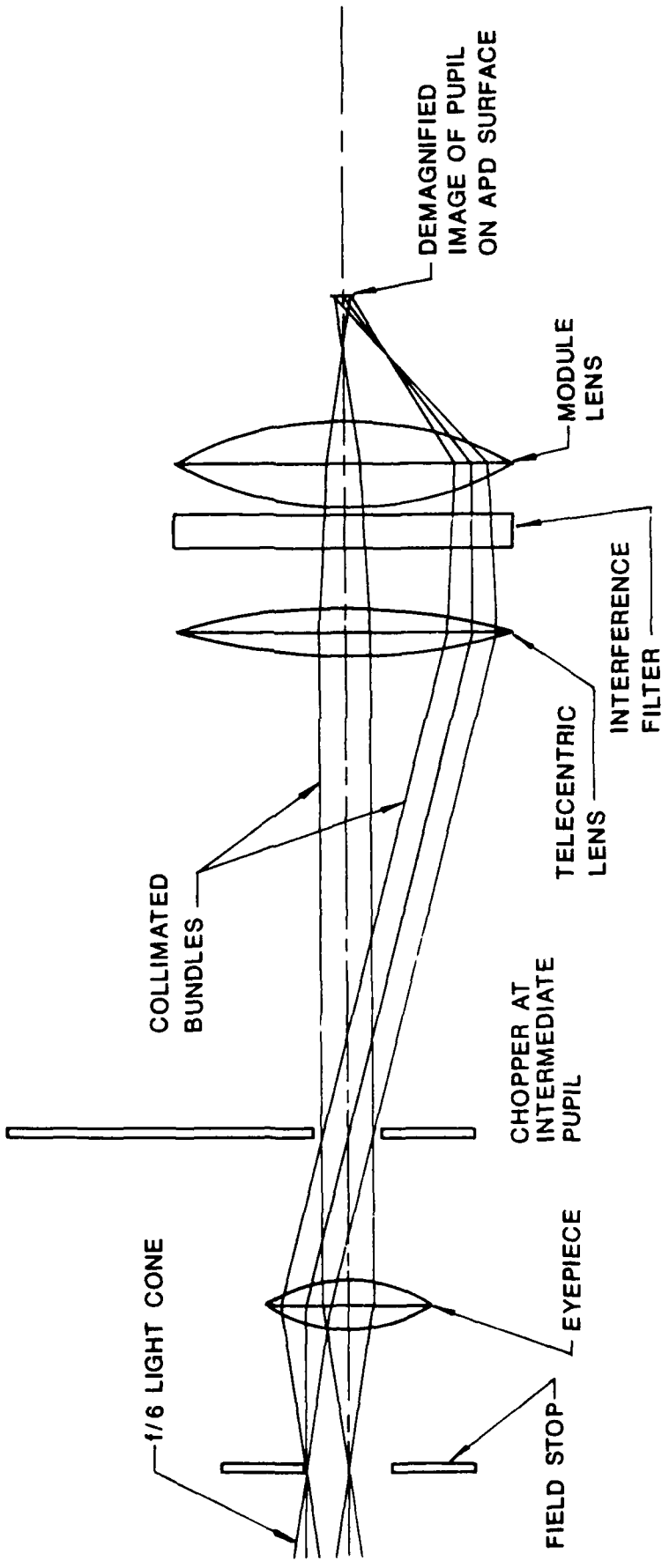

Fig. 11. 1.06 μm Leg of Dual Wavelength System.
Dichroic Filter is Not Shown.

using a piece of ground glass to locate the pupil. The pupils at the chopper and detector are real images of the primary mirror, and these images can be viewed on the ground glass. When the image on the glass is sharp the pupil has been located and the proper component can be moved into position. Pupil masks are easily centered on the pupil image and small detectors, such as avalanche photodiodes, can be properly positioned using only skylight.

D. Short Wavelength System Alignment

For LIDAR systems that have narrow receiver fields and low beam divergences, aligning the transmitter to the receiver can be like hunting for a needle in a haystack. This is especially true for the MEGALIDAR receiver with its long focal length. An alignment method that would rapidly locate the transmitter beam and optimize its location in the field of view would be of great convenience and utility.

One method would be to use a PC to steer the transmitter beam and note the location of the received signal in the field of view. Short wavelength systems could use Rayleigh scattering at a known altitude as a signal, as this signal will always be present for a short wavelength system. The PC would move a beam steering mirror in a designated search pattern until the signal was optimized.

Searching for the signal can be done with the square spiral pattern shown in Figure 12. The size of each side is incremented by an angular constant on opposite corners, the constant being less than half the size of the field stop. A reading is made at each position to see if a signal is present. Provision to exit the search loop is made if the signal is not found (i.e., PMT is not turned on).

Once the signal is located, it may be centered using the box pattern in Figure 13. The diagonal size of the box just fits within the field stop. All four corner positions are measured in rapid succession. The following logic may be used to locate the beam:

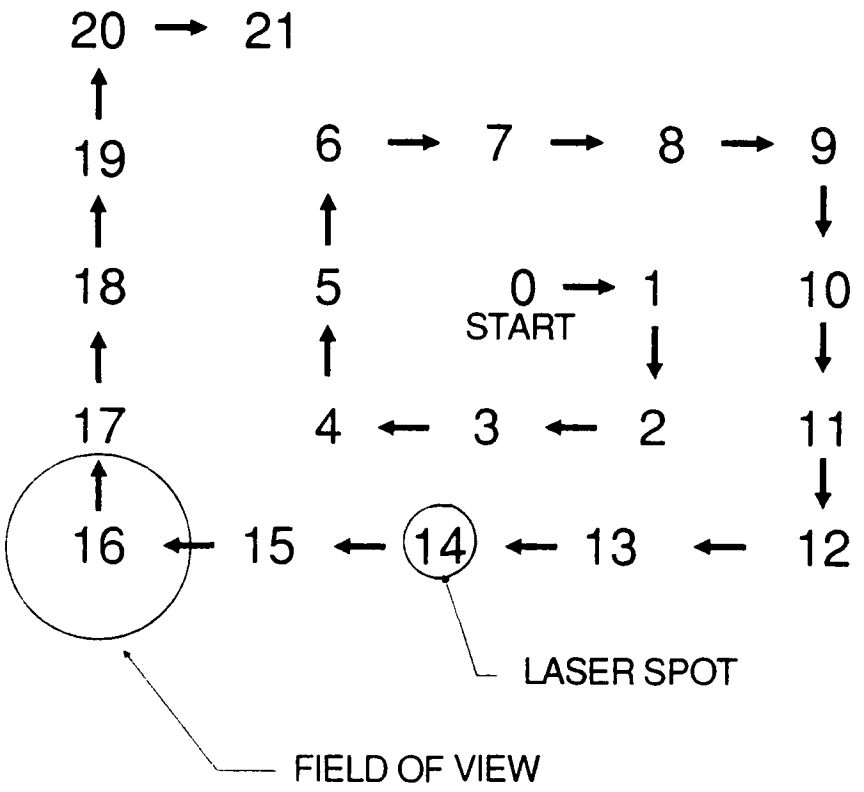

FIGURE 12. SQUARE SPIRAL SEARCH PATTERN, LASER SPOT IS FOUND AT POSITION 16

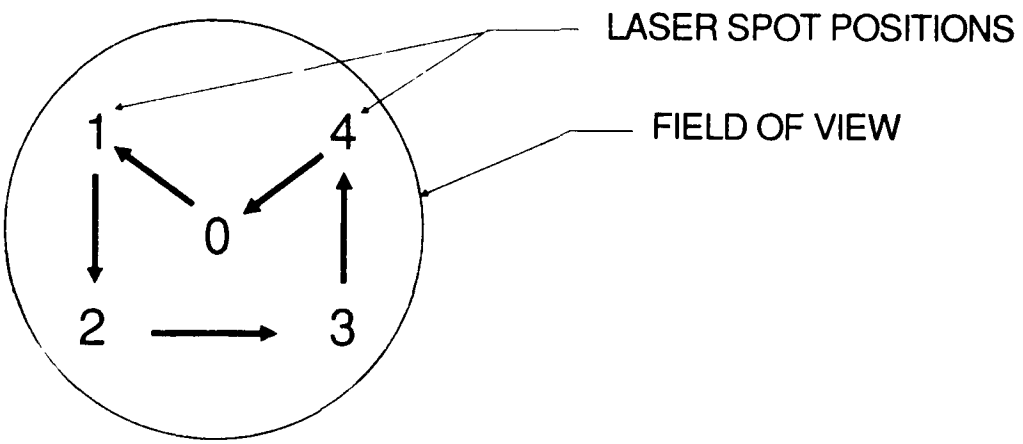

FIGURE 13. SIGNAL CENTERING PATTERN,

Signal detected at	
All positions	: centered
One corner missing	: move toward missing corner in both axes
One side missing	: move along axis toward missing side
Three corners missing	: move away from corner in both axes

If an invalid combination is detected (opposite corners missing), a retry at centering is made after returning to the original position. Several centering iterations may be made to better center the signal in the field stop. This method assumes the signal spot is a fraction of the field stop diameter, another justification for always expanding the beam. If this condition cannot be met, a larger centering aperture could be used, and once the signal was centered the smaller aperture would be moved into place.

Other alignment aids include multianode PMTs and optics for visual observation. The multianode PMTs are analogous to quadrant photodiodes. If used at prime focus, the PMT face would cover a field of several milliradians. The computer, or even the human operator, could steer the transmitter beam until the response is equal from all four PMT elements. The multianode PMT could be switched in with a folding mirror and used to initially align the transmitter to the receiver. Once completed, the folding mirror would be pulled out and final centering done with the working receiver as outlined above.

If the receiver is also equipped with an eyepiece for a human observer, the beam would be visible to the eye and could be approximately centered by hand. This method would be ideal for initial alignment after a laser or beam steering mirror was installed and the system was badly misaligned. Of course, this method would only work for visible wavelength lasers and lasers that have multiple wavelength output (doubled YAG, for example).

As the collimator facility has a vertical tube extending some 80 feet above the location for the transmitter laser (see Section VI), automatic alignment must insure the beam is traveling nearly parallel to the tube axis. If the beam is at a great enough angle to the tube axis the primary mirror will be

Accurately leveling the laser and providing the steering mirror with an angle sensor that is monitored by the computer will help keep the beam within less than a degree of the tube axis.

In addition to aligning the transmitter beam to the receiver field of view, the divergence of the transmitter beam must be checked if the beam has been expanded. Otherwise, the beam expanding telescope may be defocused, making the beam divergence unacceptably high. The focus may be checked by using a lateral shearing interferometer (LSI), a device composed of a single weak prism placed 45 degrees to the expanded laser beam. Figure 14 shows the LSI in use and the interference pattern it produces.

Some of the light entering the LSI is reflected off of the faces of the prism. The light off the back face interferes with the light reflected off the front face and produces a series of interference fringes on a screen. Horizontal fringes are produced only if plane waves are incident on the LSI, indicating the telescope is focused properly and the beam is of minimum divergence. Inclined fringes indicate spherical waves, showing the expanded laser beam is not of minimum divergence. Infrared beams may be checked in the same way if a conversion card is used to convert the IR to visible light. If the beam has been greatly expanded, the energy density on the card may be too low for it to respond. Other approaches must be taken with the LSI to check the beam focus.

E. Narrow Field MEGALIDAR Receivers at Short Wavelengths

In some circumstances, such as operation at 1.06 microns, an avalanche photodiode (APD) will have lower noise than a PMT (see Section IV). APD's have diameters in the 1-mm range, producing an extremely narrow field of view (70 microradians or less) if used at prime focus. The modular receiver design outlined earlier may be used if the telecentric lens and detector module lens demagnify the intermediate pupil at the chopper sufficiently. Placing the APD at the exit pupil insures the field will be limited only by the field stop, a component that is easily adjustable. The laser beam must be expanded considerably

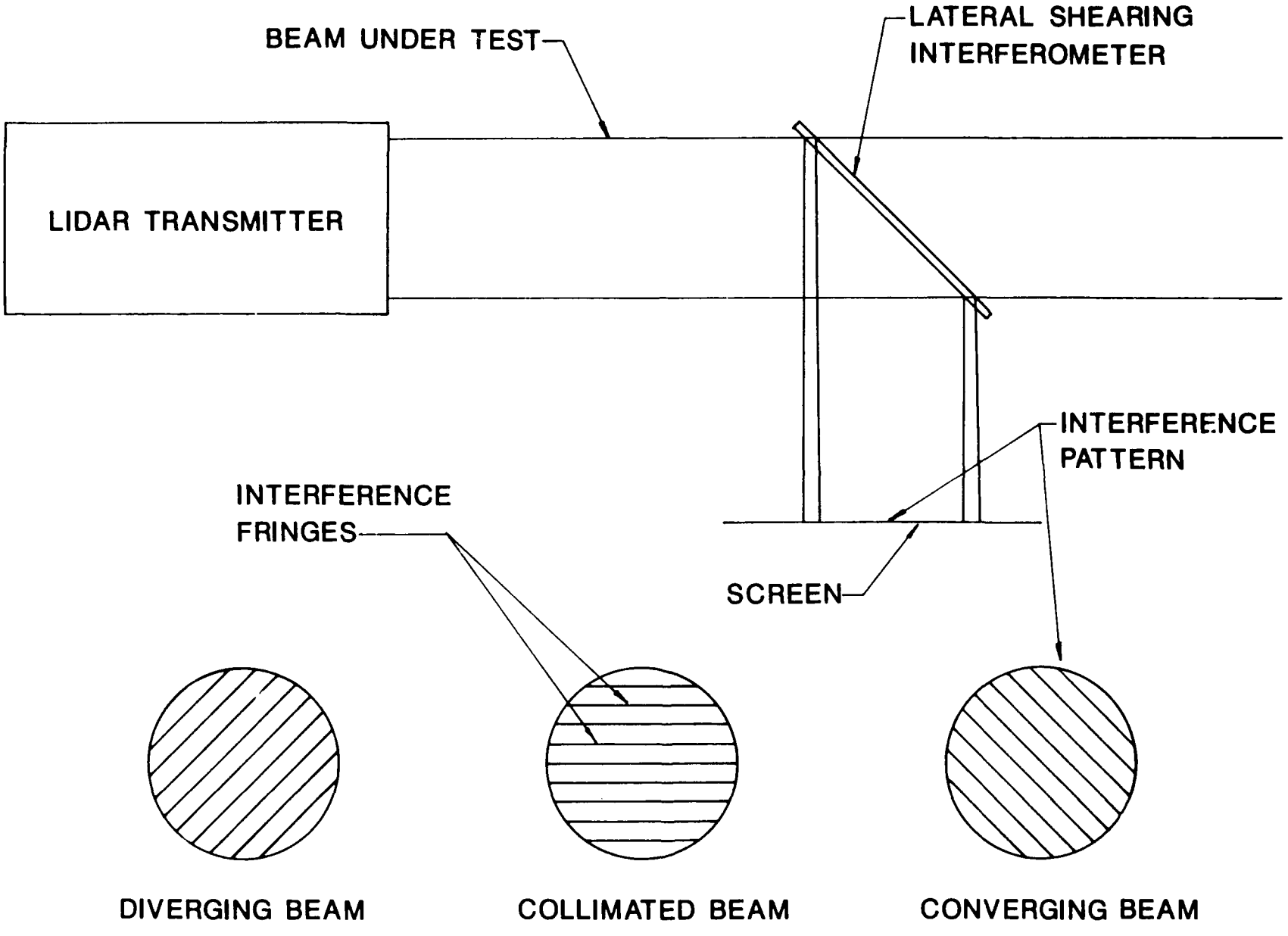

Fig. 14. Use of Lateral Shearing Interferometer.

so that the light leaving the eyepiece is diverging as slowly as possible. Otherwise, the module lens may be overfilled by the expanding light cone, or narrowband interference filters will perform poorly.

Small detectors are not the only application requiring a narrow field receiver. Lidars for Raman studies require high spectral discrimination as well as narrow fields to block the comparatively large background signal (see Sections III and IV). Fabry-Perot interferometers (FPI) may be used to provide ultra-narrow passbands (approx. 0.1 pm), and are very sensitive to off normal angles of incidence. The field stop of such a system will only be large enough to pass the signal spot. The minimum angle of incidence requirement demands that the beam be expanded as much as possible so the system spectral response is the same for all field points.

The narrow field receiver should follow the same design philosophy as the modular receiver outlined earlier. The system should be a module in a system of modules, and should be made from interchangeable modules itself. Such a configuration could be used for multiple wavelength observations with a frequency doubled Nd:YAG laser, for example. A photomultiplier would be used for the 0.532-μm wavelength, and an APD for the 1.064-μm wavelength. The receiver front end module incorporates the near-field blanking chopper required by both detectors. As the APD would require the laser beam to be expanded to minimize the exit pupil diameter, it would prove easiest to always operate with an expanded beam regardless of the receiver configuration.

As narrow-field systems require higher beam expansion than the wide-field systems described previously, reflective beam expansion telescopes are more practical than refractive systems. Off-axis mirrors, though expensive, can be fabricated in large diameters and are precise enough for use in the short wavelength region. The resulting all-reflective telescope has no central obstruction to scatter part of the laser pulse and can be made in diameters exceeding 20 inches. Refractive systems of comparable size cost as much and are more difficult to fabricate and to coat

for antireflection.

Narrow-field systems are extremely vulnerable to structural distortions of the optical system. Twisting or sagging of optical tables, mirror mounts, or of the MEGALIDAR structure itself could easily throw a system with a 70-microradian field out of alignment. Such misalignments could arise from structural distortions of the optical table, floor vibration from operators walking near the equipment, and temperature variations in the LIDAR components. Computer-aided system alignment as outlined above would be a great advantage, as it would be rapid, repeatable, and could be done as the need arises. Realigning the system would be reduced to a tiny fraction of the time it would take to do by hand.

F. Narrow Field Systems for CO_2 Laser LIDAR

CO_2 LIDAR systems bear little resemblance to the shorter wavelength systems described above. Raw beam divergences of several milliradians are typical of the TEA lasers used, and detector diameters of 200 to 300 microns are needed to reduce noise and improve time response. The small detector size translates to a tiny field of view, and beam expansion for divergence reduction requires a telescope as large as the receiver telescope. As it is rarely cost effective or practical to have two large instruments, common receiver/transmitter optics are used. In the case of the MEGALIDAR, common optics are the only possibility.

Common optics use the same telescope for both the receiver and transmitter. The laser beam must be multiplexed with the receiver path at some point in the system, requiring the use of some difference between the outgoing and incoming photons. The only difference that can be exploited without drastic power losses is polarization. A linearly polarized transmitter laser is required.

On the outgoing pass through the optical system, the linearly polarized laser pulse is converted to circular polarization by a Fresnel prism. After being scattered, the

backscattered photons return to the LIDAR with circular polarization of opposite handedness. The photons traverse the optical path in the opposite direction, and are converted back to linearly polarized photons by the Fresnel prism. Because the handedness was reversed in the scattering process, the final polarization direction is 90 degrees to the laser polarization. A beamsplitter that passes one polarization state and reflects the other can be used to separate the receiver path from the transmitter path. An example of polarization multiplexing is shown in Figure 15. The figure also illustrates a possible coherent LIDAR configuration linking the optical table to the 100-inch telescope with a collimated beam.

Polarization multiplexing can suffer losses from depolarization in the scattering process. In general, the backscattered laser light will be elliptically polarized instead of circularly polarized. When passing through the Fresnel prism the light will be converted to elliptically polarized light of different eccentricity. Only the signal component orthogonal to the laser polarization will be diverted to the detector by the polarization sensitive beamsplitter. Also, a polarizer can be used to study the depolarization of the backscattered light, but unfortunately, polarization losses may make very weak signals that have been strongly depolarized undetectable.

Common transmitter/receiver optics also reduce the alignment difficulty inherent in narrow field systems. The polarization multiplexing scheme insures the transmitter is aligned with the receiver along the path from the polarization sensitive beamsplitter to the telescope. Alignment errors between the transmitter and receiver are confined to the laser beam direction out of the laser resonator, the beamsplitter tilt, and the detector position. As these components can be located on the same table, alignment stability is much higher than the same narrow-field system with the laser widely separated from the detector.

Coherent CO_2 systems (see Section III) benefit greatly from common transmitter/receiver optics. A second laser is used as a

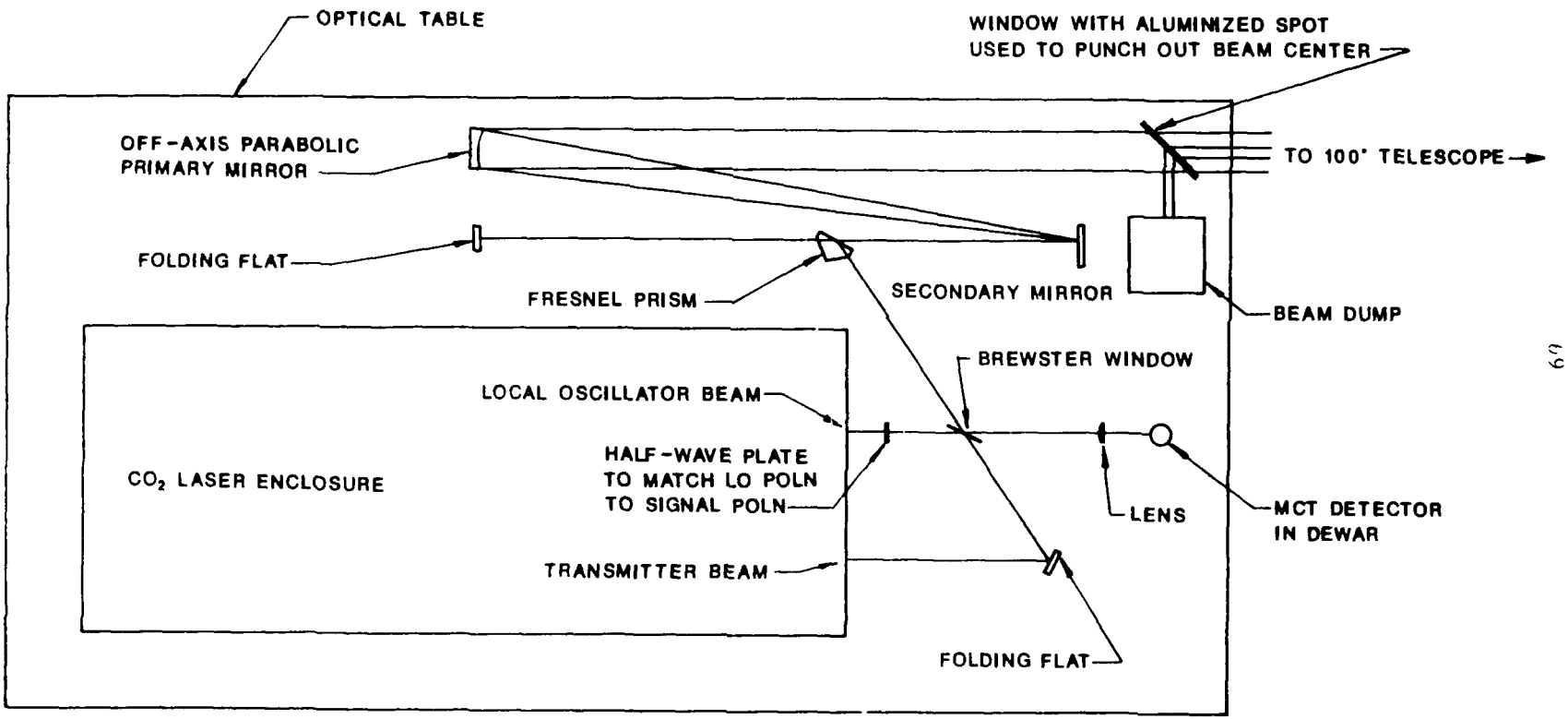

Fig. 15. Schematic of CO_2 Coherent System Showing Polarization Multiplexing.

local oscillator (LO) with a frequency shifted from the transmitter laser. When the LO field mixes with the signal field, a beat frequency equal to the frequency difference between the two is produced. The LO wavefront must match the signal wavefront as closely as possible in tilt, curvature, and polarization for maximum mixing efficiency. The polarization sensitive beamsplitter allows the signal to be co-aligned with the LO, and preserves the alignment stability of the system by locating as many components as possible on a single table.

Close tolerances on the wavefront alignment between the signal and LO make defocus a problem for coherent systems. The detector can be simultaneously at the LO and signal focal planes only for one object distance. On either side of this distance, the curvature of the signal wavefront will not match the LO wavefront. The extremely large focal length of the MEGALIDAR will accentuate this problem and may make it difficult to operate over a large range of altitudes without refocusing.

Direct detection systems require a narrowband optical filter in front of the detector. These filters typically have a 0.2-micron FWHM passbands and 85 percent or greater peak transmittance. Coherent systems do not need a narrowband filter, as the LO frequency provides the spectral discrimination. Very narrow bandwidths can be produced in this way. Spectral discrimination by the LO laser makes coherent systems sensitive to Doppler shifted signals, allowing wind velocities to be measured. (See Section III.)

Many LIDAR systems with common optics use off-axis mirrors in the telescope to avoid the backblast from the secondary mirror blocking the central part of the laser beam. If the reflected energy is not attenuated sufficiently, it will add noise to the signal, or possibly damage the detector itself. As the MEGALIDAR is an obstructed optical system the central portion of the beam should be punched out before it can reach the central obstruction. The unwanted energy is attenuated by multiple reflections inside an absorbing cavity until it is small enough not to saturate the detector. Any effects caused by stray

photons reaching the detector must be small enough to clear out by the time the pulse has reached the minimum LIDAR operating altitude. A chopper analogous to the near field blanking chopper used in short wavelength systems may also prove helpful.

As the CO_2 beam is invisible to the eye, provisions must be made to align the system using visible light. Helium-Neon lasers are ideally suited for aligning IR systems. As visible light is used for alignment, the system must use a minimum of wavelength-dependent optics. Materials like germanium are completely opaque, effectively cutting part of the system off from the alignment laser. Zinc selenide (ZnSe) is much more appropriate as it passes the He-Ne line and changes refractive index relatively little from the far IR to the visible. ZnSe is ideal for the beamsplitter and the Fresnel prism. Mirrors should be used whenever possible, especially for large components.

The small size of HgCdTe (MCT) IR detectors causes a field of view problem not present in LIDARs with shorter focal lengths and smaller apertures. Even though the beam divergence is very small after being expanded with the 100-inch mirror, the beam diameter is quite large. The beam will be nearly 100-inch in diameter for almost the entire LIDAR range, neglecting breakup from atmospheric turbulence. A spot this size can subtend an angle larger than the size of the detector's field of view for altitudes to 100 kilometers and higher. Reducing the beam expansion does not help as the secondary mirror will block more and more of the beam power as the beam gets narrower. At some point, the divergence will increase to the point where it exceeds the field of view, and the LIDAR output power will be too low. Placing the detector at the system exit pupil is a possibility, but whether a 200-micron-diameter image of the 100-inch mirror can be formed on the detector without causing other problems cannot be known without an extensive design study. Such a study is mandatory for a coherent CO_2 system.

The system alignment method outlined for short wavelength LIDARs will not work for CO_2 systems as Rayleigh scattering is minuscule near 10 micrometers. Alignment on clouds is risky as

the clouds may change characteristics within the field of view and during the alignment period. The computer will be unable to reliably optimize the returning signal, as the signal spot will cover a sizable fraction of the detector. Transmitter-to-receiver alignment must be done internal to the LIDAR itself using the He-Ne alignment lasers.

VI. Review of the Current Status of the AARI 100-Inch Collimator

A. Description of the Present Facility

The 100-inch mirror is hung on a 10-foot OD invar tube approximately 57 feet long. The invar tube is located below ground in a shaft that is approximately 75 feet deep. Above ground there is a tower that rises 72 feet so that the invar tube that supports the mirror can be raised to put the mirror at ground level. At ground level there is a cross tube 41.5 feet long and approximately 20 feet ID that has a floor and rail system to accommodate equipment under test. The invar tube in the ground shaft is enclosed by a metal vacuum vessel that is a tube 14 feet ID and approximately 65 feet long. The tower above the cross tube and the cross tube are enclosed with similar units to form a huge vessel that can be sealed and evacuated. The top of the vacuum tube is sealed with a cover that can be lifted clear of the tube and moved laterally to give a clear opening of 14 feet OD. However, the roof of the building above the tower is closed with two flap doors each 5 feet 3 inches x 11 feet 3 inches with a fixed piece across the long dimension of the opening that is 13 inches wide. Thus, there is not quite a clear view for the mirror through the roof. There are plans for a sliding door system to eliminate the center obstruction. A sketch of the facility is shown in Figure 16.

The prime focus is brought outside the vacuum vessel with a Newtonian system at a level 16 feet below the level of the cross tunnel floor. The port in the vacuum vessel is 22 inches in diameter but the clear aperture is 3 inchs in diameter. The glass window in this port has been removed. The port has a small platform attached to it to accommodate a small support for a PMT or other detector at the focus. The light beam is 48 inches from the floor. There is a large integrating sphere mounted on a overhead rail system so that it can be moved up to the port or moved back away about 8 feet. Thus there is a free volume directly in front of the port that is 8 feet x 5.3 feet x 3.75 feet.

There is a single 110-V AC circuit with two duplex outlets

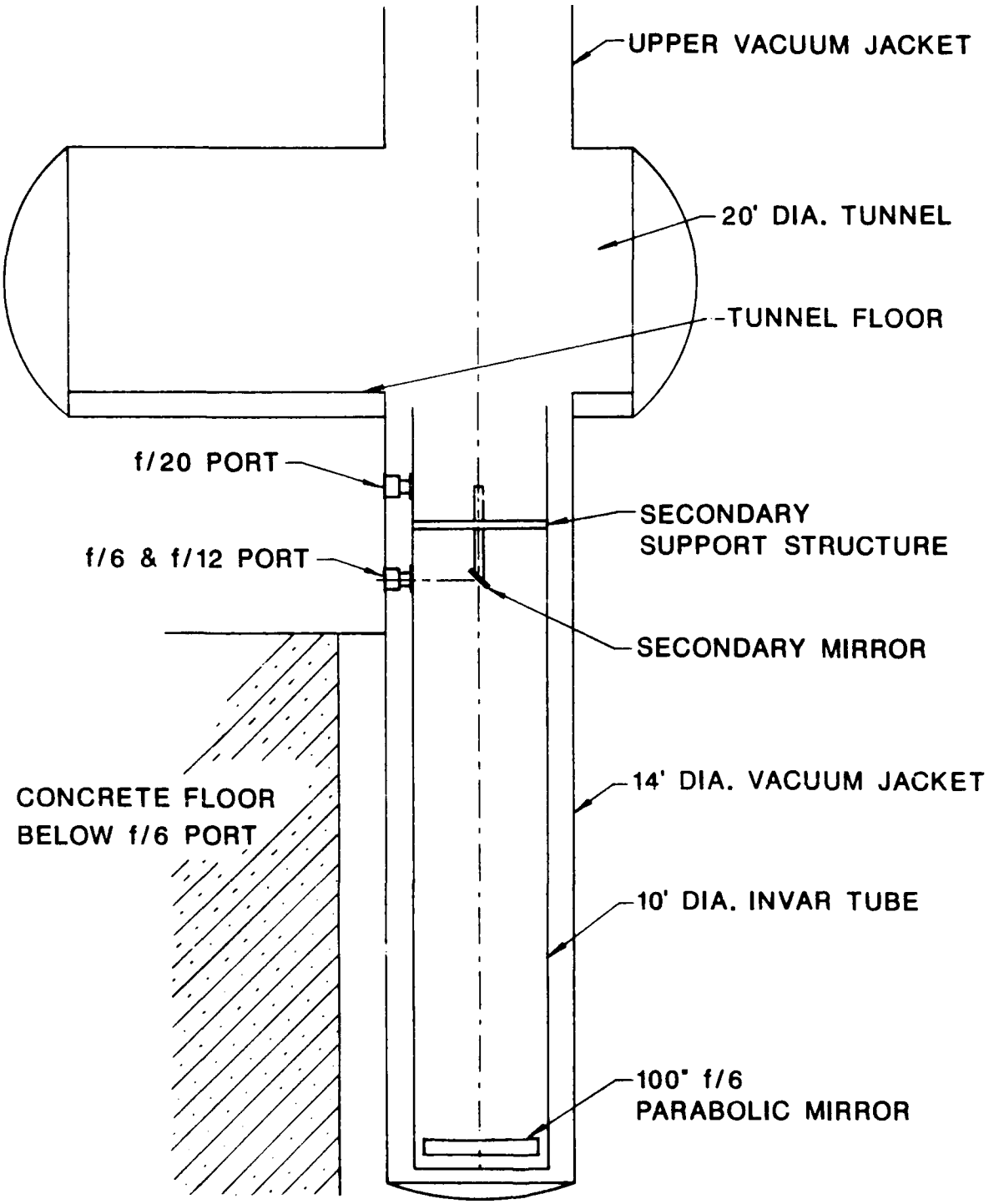

Fig. 16. Present Configuration of 100-inch Vertical Collimator

at the f/6 prime focus port. There is a distribution panel for 208 3ϕ in the tunnel.

The environmental control system for the whole collimator volume provides a constant temperature and adequate air circulation for laser cooler heat exchangers, etc. The air bag suspension and construction of the concrete structure on bedrock removes any mechanical vibration problems.

There is an optical test lab on the site so that small optical components are available as well as optics expertise. A lab and optical table are available for preassembly and alignment of LIDAR optical systems.

Liquid nitrogen is available on site as are an instrument shop and other shop facilities.

There is a building electrician that can convert circuits etc., and there is technical help from the AARI staff.

B. Present Optical Configuration of the 100 Inch Collimator

The principal component of the collimator is an f/6 paraboloidal mirror of 600 inches focal length. A 15 inch minor axis secondary mirror folds the light cone 90 degrees to a port in the vacuum jacket of the collimator. The prime focus of the mirror falls a few inches outside the vacuum jacket. Two other configurations giving f/12 and f/20 are available, but are unnecessary as the 600-inch focal length is more than long enough for LIDAR work. Figure 16 shows a simplified layout of the collimator in its present configuration.

The f/6 port is located below the cross tunnel at 45 degrees to the tunnel axis. A port for f/20 operation is positioned 7 feet above the f/6 port, also at 45 degrees to the tunnel axis. If the f/6 light cone were not folded by the secondary mirror, the focal plane would fall 7 feet above the f/6 port centerline, at the same level with the f/20 port. This position falls 7 feet below the floor of the 20-foot tunnel.

In its present configuration the 100 inches can be used as a short wavelength LIDAR (fundamental, doubled, or tripled Nd:YAG, for example) by placing the laser in the 20-foot tunnel and

folding the beam upward with a flat mirror. A receiver unit can be attached directly to the f/6 port, and all data collection equipment may be positioned on the floor near the receiver.

C. Special Considerations for the MEGALIDAR

While the 100 inches offers superior light collecting ability over existing LIDAR receivers, it is not without its problems. The 600-inch focal length gives the receiver a narrow field of view even for large photomultiplier tubes. Very small detectors, such as MCT IR detectors, will have fields of view of 30 microradians or less. These narrow fields can make the resulting LIDAR impossible to align if the optical design and alignment techniques do not allow for them. The following table lists various field stop (or detector) sizes and the resulting fields of view for the MEGALIDAR when the field stop is at the f/6 focus.

Field Stop Diameter	Field of View
20.0 mm	1.3 mrad
2.0 mm	0.1 mrad
0.5 mm	0.03 mrad
0.2 mm	0.01 mrad

For reference, 1 mrad = 3.4 arcminutes and 0.01 mrad = 2 arcseconds. The last two entries are typical sizes for MCT detectors.

The large focal length greatly accentuates a problem inherent in most LIDARs: defocus for varying object distances. As the laser pulse travels upward, each molecule and particle in its path will act as a point source of scattered light. The receiver telescope will focus the collected light behind the plane where light from a source at infinity would be focused. A receiver system focused for infinity will form a large spot of light on the field stop or detector for objects in the near field. This spot will overfill the field stop or detector causing severe losses in collected power. Small detectors may fall within the shadow produced by the secondary mirror, receiving no light at all. Coherent systems will suffer because the defocused signal wavefront will not match the local oscillator wavefront, reducing

mixing efficiency. The table below illustrates defocus for the MEGALIDAR receiver focused for infinity, detector at the f/6 focus, and a point source on the axis.

Source Distance	Defocus Distance	Spot Diameter
1 km	236 mm	40.0 mm
5 km	47 mm	8.0 mm
10 km	23 mm	4.0 mm
20 km	12 mm	2.0 mm
50 km	5 mm	0.8 mm
100 km	2 mm	0.4 mm

The defocus distance is the distance the light comes to a focus behind the infinite-object-distance plane. The spot diameter is the diameter of the converging light cone in the infinite-object-distance plane. From the entries in the spot diameter column, defocus presents a particularly serious problem for systems using tiny detectors, such as MCT. Even for systems using large PMT's the near-field defocus will overfill the field stop used for limiting background power.

There are partial solutions for the narrow field of view and for defocus. The field can be opened up somewhat by a single lens, called a telecompressor, positioned before the focus of the 100-inch paraboloid. This lens will effectively shorten the focal length of the primary mirror and produce a larger field of view. However, this can be used to advantage only in systems not suffering from excess background power. Since the effective focal length is shorter, defocus is also reduced by the use of this same lens. Restricting MEGALIDAR operation to altitudes greater than 20 km (or short intervals at lower altitudes) will reduce defocus as well.

The large collecting area of the 100" mirror leads to a near-field return problem. Enough laser light from near-field targets (the air, for example) will be collected to drive the detector into saturation, temporarily blinding the LIDAR. Turning the detector off until the pulse has traveled to a safe distance is not a complete solution as the collected photons will still produce charge carriers in the detector. These charge carriers will add noise to the signal after the detector is

turned on again, degrading the signal. A better solution is to block the detector with a rapidly rotating chopper blade. All backscattered photons are prevented from reaching the detector surface until the pulse has reached a safe altitude.

When the pulse has climbed far enough for the signal to drop to photon counting levels, post-pulse laser emissions can cause an intolerable background level. The flash lamps in a Nd:YAG laser are an example, as they may still be glowing long after the flash, or they may be kept "simmering" in readiness for the next flash. The unwanted output may be reduced by placing the laser in a light-tight box and using a chopper to cover the hole the beam passes through. Large diameter beams (1 cm) may use two counter-rotating synchronized choppers to close the hole off twice as fast as a single chopper. The two blades would provide a better blocking effect as well.

Enclosing the beam in a long, well baffled tube will also help reduce stray flashlamp light. The stray light must travel at large angles to the laser axis to get around the chopper blades. It will bounce many times among the tube baffles before it can get to the end of the tube, by which time most of it will have been absorbed in the tube walls. Such a tube could be placed between the laser and the steerable mirror used to direct the beam upward.

D. Modification to the Collimator for LIDAR

The present configuration is suitable only for short wavelength LIDAR systems with the receiver d[illegible]s outlined in Section V. When a CO_2 system is installed, modifications to the present secondary mirror assembly must be made to accommodate both CO_2 and short wavelength operation. Switching from CO_2 to shorter wavelengths would be done quickly with a minimum of change to the system so measurements can be made in both regions in rapid succession.

In order to use the 100-inch mirror over such a large wavelength region an all-reflective design is required. Using all-reflective optics allows wavelength dependent components of the

system (such as lenses) to be optimized for their wavelength region alone. The simplest wavelength independent configuration is the Mersennes arrangement consisting of a concave parabolic primary and a convex parabolic secondary. The separation of the two mirrors is adjustable to place the image formed by one mirror at the focus of the other. The arrangement can be used as a beam expander for a CO_2 system as well as a receiver for any system.

Since the system is rotationally symmetric about the collimator axis and light enters and leaves the system nearly parallel to the optic axis, a third mirror is needed to direct the light into or out of the system. The most useful configuration is shown in Figure 17, where a perforated flat is used to fold the light cone onto the secondary. When operating as a receiver, light exiting the system can travel vertically to the cross tunnel, or be folded over to the f/6 station by a small flip mirror behind the perforated mirror.

When using the telescope as a beam expander for a CO_2 system, we should remember that the system changes its effective focal length when the laser beam changes its angle with respect to the telescope's optic axis. This causes the beam to change divergence as the beam direction changes, possibly growing too large to fit within the receiver field of view. The beam direction would change only during alignment, so the focus of the telescope must be checked every time the system is adjusted. The focal setting may be changed by translating the secondary mirror along the optic axis.

Only CO_2 systems need to use the 100-inch mirror as part of a beam expanding system. Short wavelength systems can have their beams expanded by a separate telescope and directed upward by a flat steering mirror positioned over the primary mirror aperture. The steering mirror should be permanently mounted on a spider in the cross tunnel, as the transmitter will always be located in the tunnel. Figure 17 shows this steering mirror on its support spider. A second folding mirror used to direct a CO_2 beam down to the 100-inch telescope may be inserted in the housing beneath the large steering mirror.

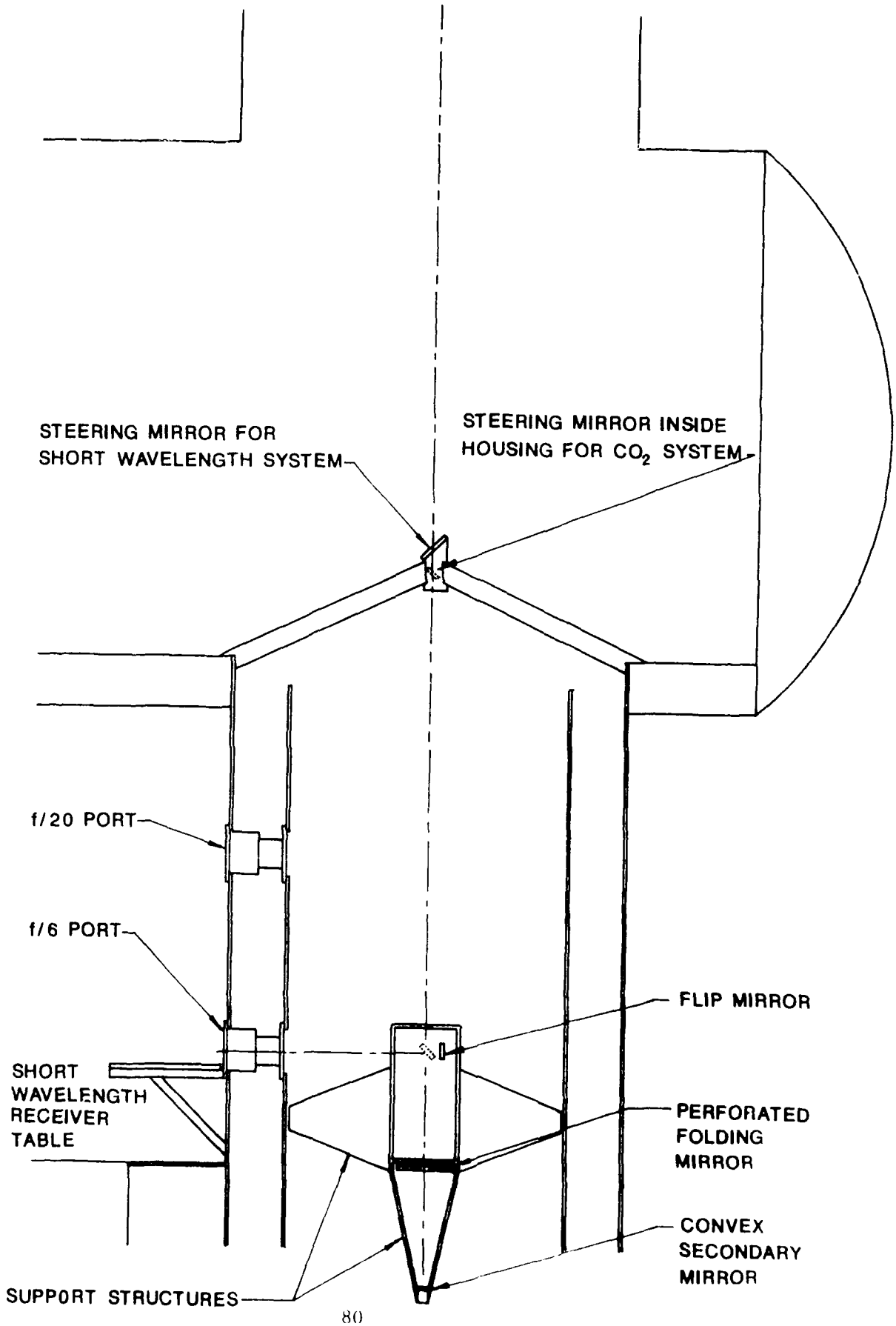

Fig. 17. Modifications to 100-inch Collimator.
Only Section from Secondary Mirror is Shown.

VII. Summary and Recommendations

This report is a study of the feasibility of converting the 100-inch collimator at Wright-Patterson AFB into a LIDAR atmospheric remote sensing system which is referred to as the MEGALIDAR. In light of the present and future needs of the Air Force for more appropriate characterization of the atmosphere, the authors suggest four specific types of measurement programs that could be initiated: cloud characterization studies, studies of the stratospheric and mesospheric aerosols, measurement of ozone concentrations, measurement of density and temperature profiles in the middle atmosphere and their time variation. Atmospheric molecular scattering profiles are presented that are the results of simulations of the performance of the collimator under various conditions of laser power and received signal averaging time. The profiles are a series of graphs that show the photoelectron per measurement interval produced by a photomultipier tube in a receiver attached to the collimator versus the altitude of the volume that produced the backscattering light collected by the collimator. The profiles can be used to obtain a rough estimate of the range of the MEGALIDAR under the conditions of the simulations and thus serve as an aid in evaluating proposed MEGALIDAR measurements.

A survey of the various types of LIDAR measurement systems and their performance requirements is presented. The systems discussed are: elastic scattering LIDAR, Differential Absorption LIDAR (DIAL), Raman scattering LIDAR, fluorescence LIDAR and CO_2 coherent LIDAR. The various atmospheric parameters that can be measured using these systems are discussed to show that it is necessary to have a multi-LIDAR capability for the MEGALIDAR in order to meet the demands of the measurement programs required to meet Air Force needs.

A discussion of the characteristics of available instruments to implement the various LIDAR systems is provided. This includes a description of available laser transmitters and detectors for the spectral regions used for LIDAR. Consideration is given to special features of the MEGALIDAR that include an estimate of the maximum possible range, filtering and beam chopping. Methods

of noise reduction and data handling are also presented.

The LIDARS are also classified by optical design requirements. These include a wide field MEGALIDAR receiver for short wavelengths, a narrow field MEGALIDAR receiver for short wavelengths and narrow field systems for CO_2 LIDAR. Details of modular designs for each of these systems are given. Design enhancements for narrow spectral bandwidths and placement of a mechanical chopper for truncation of the received beam are presented.

A review of the current status of the collimator is provided. This includes a description of the present physical facilities and an assessment of how they would accommodate the requirements for placement of the LIDAR systems. Consideration is also given to ancillary support such as machine shop, facilities and space for preliminary assembly of the systems before they are put on the collimator, and a laboratory for test of optical components. The present optical configuration of the collimator is also evaluated for application to MEGALIDAR. An alignment procedure for this kind of a narrow field of view instrument is proposed. A modifications of the optics of the collimator to accommodate a CO_2 LIDAR system are also presented.

The most obvious scientific aim of the MEGALIDAR that could contribute to the mission of the Air Force is to provide characterizations of the middle atmosphere that are not available in any other way. In addition, The MEGALIDAR could contribute in the broad areas of the development of instruments for sensing and correcting for the effects of the atmosphere and the development of methods of data collection, analyses and presentation. The MEGALIDAR is unique not only because it will have the largest mirror receiver in the world, but because it is housed in a controlled environment that reduces the effects of temperature variations and mechanical vibrations to a negligible level. The structure around the mirror is large enough to house almost unlimited arrangements of transmitter and receiver optics. The proximity of high level technical support from the whole of Wright-Patterson make its support facilities unparalleled by other LIDAR facilities.

◎U.S.Government Printing Office: 1989 648 056/04481